NGA Ground Motion Model for the Geometric Mean Horizontal Component of PGA, PGV, PGD and 5% Damped Linear Elastic Response Spectra for Periods Ranging from 0.01 to 10 s

Kenneth W. Campbell,[a] M.EERI, **and Yousef Bozorgnia,**[b] M.EERI

We present a new empirical ground motion model for PGA, PGV, PGD and 5% damped linear elastic response spectra for periods ranging from 0.01–10 s. The model was developed as part of the PEER Next Generation Attenuation (NGA) project. We used a subset of the PEER NGA database for which we excluded recordings and earthquakes that were believed to be inappropriate for estimating free-field ground motions from shallow earthquake mainshocks in active tectonic regimes. We developed relations for both the median and standard deviation of the geometric mean horizontal component of ground motion that we consider to be valid for magnitudes ranging from 4.0 up to 7.5–8.5 (depending on fault mechanism) and distances ranging from 0–200 km. The model explicitly includes the effects of magnitude saturation, magnitude-dependent attenuation, style of faulting, rupture depth, hanging-wall geometry, linear and nonlinear site response, 3-D basin response, and inter-event and intra-event variability. Soil nonlinearity causes the intra-event standard deviation to depend on the amplitude of PGA on reference rock rather than on magnitude, which leads to a decrease in aleatory uncertainty at high levels of ground shaking for sites located on soil. [DOI: 10.1193/1.2857546]

INTRODUCTION

The empirical ground motion model (attenuation relation) presented in this paper represents the culmination of a four-year multidisciplinary study sponsored by the Pacific Earthquake Engineering Research Center (PEER) and referred to as the Next Generation Attenuation (NGA) Ground Motion Project (Power et al. 2008, this volume). This new ground motion model is considered to supersede our existing ground motion models for peak ground velocity (PGV) as documented in Campbell (1997) and for peak ground acceleration (PGA) and 5% damped pseudo-absolute response spectral acceleration (PSA) as documented in Campbell and Bozorgnia (2003). We do not have an existing model for peak ground displacement (PGD) that we can compare with our new

[a] ABS Consulting/EQECAT, 1030 NW 161st Pl., Beaverton, OR 97006-6337; E-mail: kcampbell@eqecat.com
[b] Pacific Earthquake Eng. Research Center, 325 Davis Hall, University of California, Berkeley, CA 94720-1792

Earthquake Spectra, Volume 24, No. 1, pages 139–171, February 2008;

model. The NGA models represent a major advancement in ground motion prediction made possible by the extensive update of the PEER strong motion database and the supporting studies on 1-D ground motion simulation, 1-D site response, and 3-D basin response sponsored by the NGA project (Power et al. 2008, this volume). This paper provides a brief description of the database, functional forms, and analyses that went into the development of our new NGA ground motion model. This is followed by a comparison of our new model with our previous models. Additional documentation of our NGA ground motion model is given in Campbell and Bozorgnia (2007).

DATABASE

The database used for this study was a subset of the updated PEER strong motion database (Chiou and Silva 2008, this volume), sometimes referred to simply as the NGA database. The general criteria that we used to select this subset was intended to meet our requirements that the earthquake be located within the shallow continental lithosphere (i.e., the Earth's crust) in a region considered to be tectonically active, that the recording be located at or near ground level and exhibit no known embedment or topographic effects, that the earthquake have enough recordings to reliably represent the mean horizontal ground motion (especially for small-magnitude events), and that the earthquake or the recording be considered reliable according to criteria set forth in Campbell and Bozorgnia (2007).

Specific application of the above general criteria resulted in the exclusion of the following data from the subset: (1) any recording with only one horizontal component or only a vertical component; (2) any recording site without a measured or estimated 30-m shear-wave velocity (V_{S30}); (3) any earthquake without a rake angle, focal mechanism, or plunge of the maximum compressive stress (P) and minimum compressive stress (T) axes; (4) any earthquake with the hypocenter or a significant amount of the fault rupture located in the lower crust, in an oceanic plate, or in a stable continental region; (5) any LDGO recording from the 1999 Düzce, Turkey, earthquake that was considered to be unreliable based on its spectral shape; (6) any recording from instruments designated as low quality ("D") from the 1999 Chi-Chi, Taiwan, earthquake; (7) any earthquake considered to be an aftershock and not a "triggered" event such as the 1992 Big Bear earthquake; (8) any earthquake considered to have too few recordings in relation to its magnitude, which we define as an earthquake with (a) $\mathbf{M} < 5.0$ and $N < 5$, (b) $5.0 \leq \mathbf{M} < 6.0$ and $N < 3$, or (c) $6.0 \leq \mathbf{M} < 7.0$, $R_{RUP} > 60$ km and $N < 2$, where $\mathbf{M}$ is moment magnitude, N is the number of recordings, and R_{RUP} is the closest distance to coseismic rupture (note that singly recorded earthquakes with $\mathbf{M} \geq 7.0$ and $R_{RUP} \leq 60$ km were retained because of their significance); (9) any recording considered to represent non-free-field site conditions, which we define as an instrument located (a) in the basement of a building, (b) below the ground surface, or (c) on a dam except the abutment; and (10) any recording with known topographic effects such as the Pacoima Dam upper left abutment and the Tarzana Cedar Hill Nursery. Additional details are given in Campbell and Bozorgnia (2007).

Application of the above criteria resulted in the selection of 1561 recordings from 64 earthquakes with moment magnitudes ranging from 4.3–7.9 and rupture distances ranging from 0.1–199 km. Table 1 presents a summary of these earthquakes. A complete list of the selected earthquakes and recording stations are given in Appendix A of Campbell and Bozorgnia (2007). The distribution of the recordings with respect to magnitude and distance is shown in Figure 1.

GROUND MOTION MODEL

The functional forms used to define our NGA ground motion model were developed or confirmed using classical data exploration techniques, such as analysis of residuals. Candidate functional forms were either developed by us or evaluated from those available from the literature or proposed during the NGA project using numerous iterations to capture the observed trends in the recorded ground motion data. Final functional forms were selected according to (1) their sound seismological basis; (2) their unbiased residuals; (3) their ability to be extrapolated to values of magnitude, distance, and other explanatory variables that are important for use in engineering and seismology; and (4) their simplicity, although this latter consideration was not an overriding factor. The third criterion was the most difficult to achieve because the data did not always allow the functional forms of some explanatory variables to be developed empirically. In such cases, theoretical constraints were used to define the functional forms based on supporting studies sponsored by the NGA project (Power et al. 2008, this volume).

During the model development phase of the study, regression analyses were performed in two stages for a limited set of oscillator periods, T, using the two-stage regression procedure summarized by Boore et al. (1997). However, in our application of this procedure, each step utilized nonlinear rather than linear regression analysis. In Stage 1, the mathematical terms involving individual recordings (the intra-event terms f_{dis}, f_{hng}, f_{site}, and f_{sed}) were fit by the method of nonlinear least squares using all of the recordings. In Stage 2, the mathematical terms common to all recordings of a specific earthquake (the inter-event terms f_{mag} and f_{flt}) were fit by the method of weighted least squares using the event terms from Stage 1 as the "data." Each event term was assigned a weight that was inversely proportional to its calculated variance from Stage 1. This two-stage analysis allowed us to decouple the intra-event and inter-event terms, which stabilized the regression analysis and allowed us to independently evaluate and model magnitude scaling effects at large magnitudes. Once the functional forms for all of the mathematical terms were established, a series of iterative random-effects regression analyses (Abrahamson and Youngs 1992) were performed for the entire range of periods in order to derive a smoothed set of model coefficients and to calculate the final values of the inter-event and intra-event standard deviations.

DEFINITION OF GROUND MOTION COMPONENTS

The ground motion component used in the NGA models is not the traditional geometric mean of the two "as-recorded" horizontal components that has been used in past studies. The principle drawback of the old geometric mean is its dependence on the orientation of the sensors as installed in the field. The new geometric mean, referred to as "GMRotI50" by Boore et al. (2006), is independent of both sensor orientation and oscillator period and, as a result, represents a more robust horizontal ground motion com-

Table 1. List of earthquakes used in the analysis

EQ No.	Earthquake Name	Year	**M**	Style of Faulting	No. of Rec.	R_{RUP} (km) Min.	Max.
12	Kern County, Calif.	1952	7.36	Reverse	1	117.75	117.75
25	Parkfield, Calif.	1966	6.19	Strike-slip	4	9.58	17.64
29	Lytle Creek, Calif.	1970	5.33	Reverse	10	15.27	106.63
30	San Fernando, Calif.	1971	6.61	Reverse	33	19.30	193.91
31	Managua, Nicaragua	1972	6.24	Strike-slip	1	4.06	4.06
140	Sitka, Alaska	1972	7.68	Strike-slip	1	34.61	34.61
40	Friuli, Italy	1976	6.50	Reverse	5	15.82	102.16
41	Gazli, USSR	1976	6.80	Reverse	1	5.46	5.46
141	Caldiran, Turkey	1976	7.21	Strike-slip	1	50.82	50.82
46	Tabas, Iran	1978	7.35	Reverse	7	2.05	194.55
48	Coyote Lake, Calif.	1979	5.74	Strike-slip	10	3.11	33.83
49	Norcia, Italy	1979	5.90	Normal	3	7.37	36.47
50	Imperial Valley, Calif.	1979	6.53	Strike-slip	33	0.07	50.10
142	St Elias, Alaska	1979	7.54	Reverse	2	26.46	80.00
53	Livermore, Calif.	1980	5.80	Strike-slip	5	20.53	57.38
55	Anza (Horse Canyon), Calif.	1980	5.19	Strike-slip	5	15.57	43.44
56	Mammoth Lakes, Calif.	1980	6.06	Normal	3	4.67	15.46
64	Victoria, Mexico	1980	6.33	Strike-slip	4	7.27	39.30
68	Irpinia, Italy	1980	6.90	Normal	12	8.18	59.63
72	Corinth, Greece	1981	6.60	Normal	1	10.27	10.27
73	Westmorland, Calif.	1981	5.90	Strike-slip	6	6.50	19.37
76	Coalinga, Calif.	1983	6.36	Reverse	45	8.41	55.77
87	Borah Peak, Idaho	1983	6.88	Normal	2	83.00	84.80
90	Morgan Hill, Calif.	1984	6.19	Strike-slip	27	0.53	70.93
91	Lazio-Abruzzo, Italy	1984	5.80	Normal	5	18.89	51.29
97	Nahanni, Canada	1985	6.76	Reverse	3	4.93	9.60
98	Hollister, Calif.	1986	5.45	Strike-slip	3	14.31	17.14
101	N. Palm Springs, Calif.	1986	6.06	Reverse	31	4.04	78.09
102	Chalfant Valley #1, Calif.	1986	5.77	Strike-slip	5	6.39	24.45
103	Chalfant Valley #2, Calif.	1986	6.19	Strike-slip	11	7.58	51.98
111	New Zealand	1987	6.60	Normal	2	16.09	68.74
113	Whittier Narrows #1, Calif.	1987	5.99	Reverse	109	14.50	103.90
114	Whittier Narrows #2, Calif.	1987	5.27	Reverse	10	14.02	27.80
115	Elmore Ranch, Calif.	1987	6.22	Strike-slip	1	17.59	17.59
116	Superstition Hills, Calif.	1987	6.54	Strike-slip	11	0.95	27.00
118	Loma Prieta, Calif.	1989	6.93	Reverse	77	3.85	117.08
119	Griva, Greece	1990	6.10	Normal	1	29.20	29.20
143	Upland, Calif.	1990	5.63	Strike-slip	3	11.71	75.46
144	Manjil, Iran	1990	7.37	Strike-slip	7	12.56	174.55
145	Sierra Madre, Calif.	1991	5.61	Reverse	8	10.36	39.81
121	Erzican, Turkey	1992	6.69	Strike-slip	1	4.38	4.38

Table 1. (cont.)

EQ No.	Earthquake Name	Year	**M**	Style of Faulting	No. of Rec.	R_{RUP} (km) Min.	Max.
123	Cape Mendocino, Calif.	1992	7.01	Reverse	6	6.96	41.97
125	Landers, Calif.	1992	7.28	Strike-slip	67	2.19	190.05
126	Big Bear, Calif.	1992	6.46	Strike-slip	38	8.40	147.90
152	Little Skull Mtn., Nevada	1992	5.65	Normal	8	16.06	100.16
127	Northridge, Calif.	1994	6.69	Reverse	149	5.19	147.55
129	Kobe, Japan	1995	6.90	Strike-slip	22	0.27	158.61
130	Kozani, Greece	1995	6.40	Normal	3	19.54	79.38
134	Dinar, Turkey	1995	6.40	Normal	2	3.36	44.15
136	Kocaeli, Turkey	1999	7.51	Strike-slip	22	4.83	180.24
137	Chi-Chi, Taiwan	1999	7.62	Reverse	381	0.32	169.90
138	Duzce, Turkey	1999	7.14	Strike-slip	14	6.58	188.70
158	Hector Mine, Calif.	1999	7.13	Strike-slip	78	11.66	198.13
160	Yountville, Calif.	2000	5.00	Strike-slip	24	14.15	96.20
161	Big Bear, Calif.	2001	4.53	Strike-slip	43	24.32	92.73
162	Mohawk Valley, Calif.	2001	5.17	Strike-slip	6	68.66	127.29
163	Anza, Calif.	2001	4.92	Strike-slip	72	18.45	134.20
164	Gulf of California, Mexico	2001	5.70	Strike-slip	11	77.33	134.43
165	Baja, Mexico	2002	5.31	Strike-slip	9	42.79	99.68
166	Gilroy, Calif.	2002	4.90	Strike-slip	34	10.51	131.53
167	Yorba Linda, Calif.	2002	4.27	Strike-slip	12	14.60	38.29
168	Nenana Mtn., Alaska	2002	6.70	Strike-slip	5	104.73	199.27
169	Denali, Alaska	2002	7.90	Strike-slip	9	2.74	164.66
170	Big Bear City, Calif.	2003	4.92	Strike-slip	36	25.58	147.08

ponent. It was found to have a value that is on average within a few percent of the old geometric mean (Beyer and Bommer 2006; Boore et al. 2006; Bozorgnia et al. 2006; Campbell and Bozorgnia 2007). In some engineering applications it is necessary to calculate the median and aleatory uncertainty of the arbitrary horizontal component (Baker and Cornell 2006). The median estimate of this component is equivalent to the median estimate of the traditional geometric mean (Beyer and Bommer 2006); therefore, it also has an average value that is within a few percent of the new geometric mean (Figure 2; Beyer and Bommer 2006; Campbell and Bozorgnia 2007; Watson-Lamprey and Boore 2007). However, as discussed latter in the paper, the variance of the arbitrary horizontal component must be increased by the variance of the component-to-component variability between the two horizontal components of the recording.

Engineers have recently shown an increased interest in the relationship between the geometric mean horizontal component used in many ground motion models and other higher-amplitude horizontal components. We addressed this issue by performing a statistical analysis of the logarithmic ratio between several of these alternative horizontal ground motion components and the new geometric mean. Figure 2 shows these results

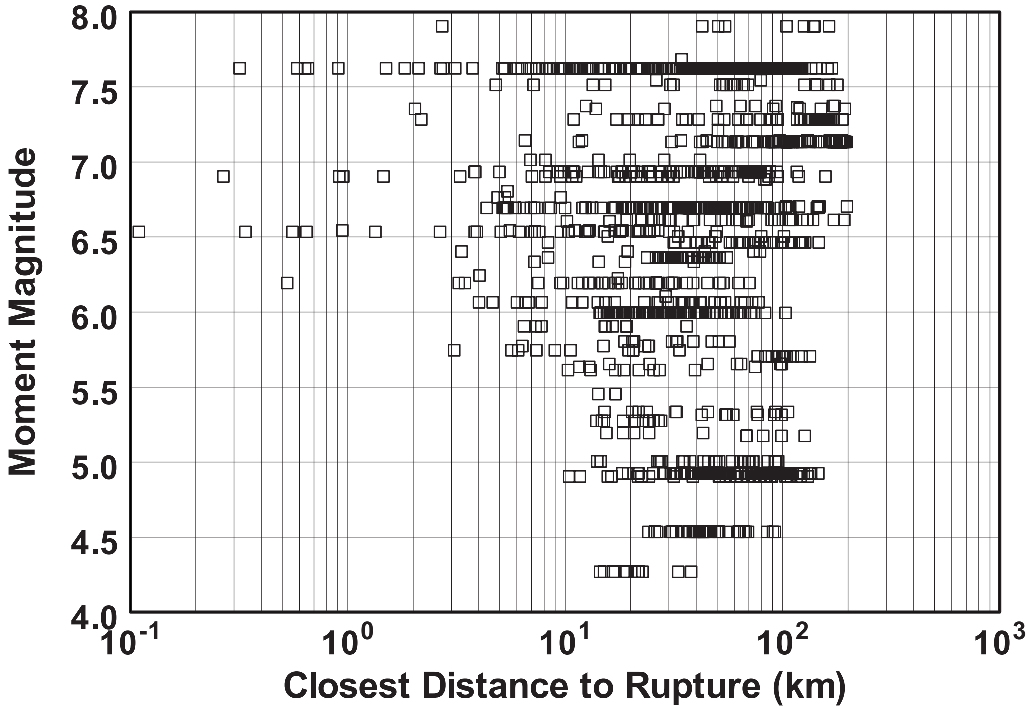

Figure 1. Distribution of recordings with respect to moment magnitude (**M**) and rupture distance (R_{RUP}) for the database used in this study.

for the maximum arbitrary (as-recorded) horizontal component, the maximum rotated horizontal component, and the strike-normal component. Exact definitions of these components along with additional statistical correlations and tabulated ratios are provided by Beyer and Bommer (2006), Campbell and Bozorgnia (2007), and Watson-Lamprey and Boore (2007).

MEDIAN GROUND MOTION MODEL

The median estimate of ground motion can be calculated from the general equation

$$\ln \hat{Y} = f_{mag} + f_{dis} + f_{flt} + f_{hng} + f_{site} + f_{sed} \tag{1}$$

where the magnitude term is given by the expression

$$f_{mag} = \begin{cases} c_0 + c_1\mathbf{M}; & \mathbf{M} \leqslant 5.5 \\ c_0 + c_1\mathbf{M} + c_2(\mathbf{M} - 5.5); & 5.5 < \mathbf{M} \leqslant 6.5 \\ c_0 + c_1\mathbf{M} + c_2(\mathbf{M} - 5.5) + c_3(\mathbf{M} - 6.5); & \mathbf{M} > 6.5 \end{cases} \tag{2}$$

the distance term is given by the expression

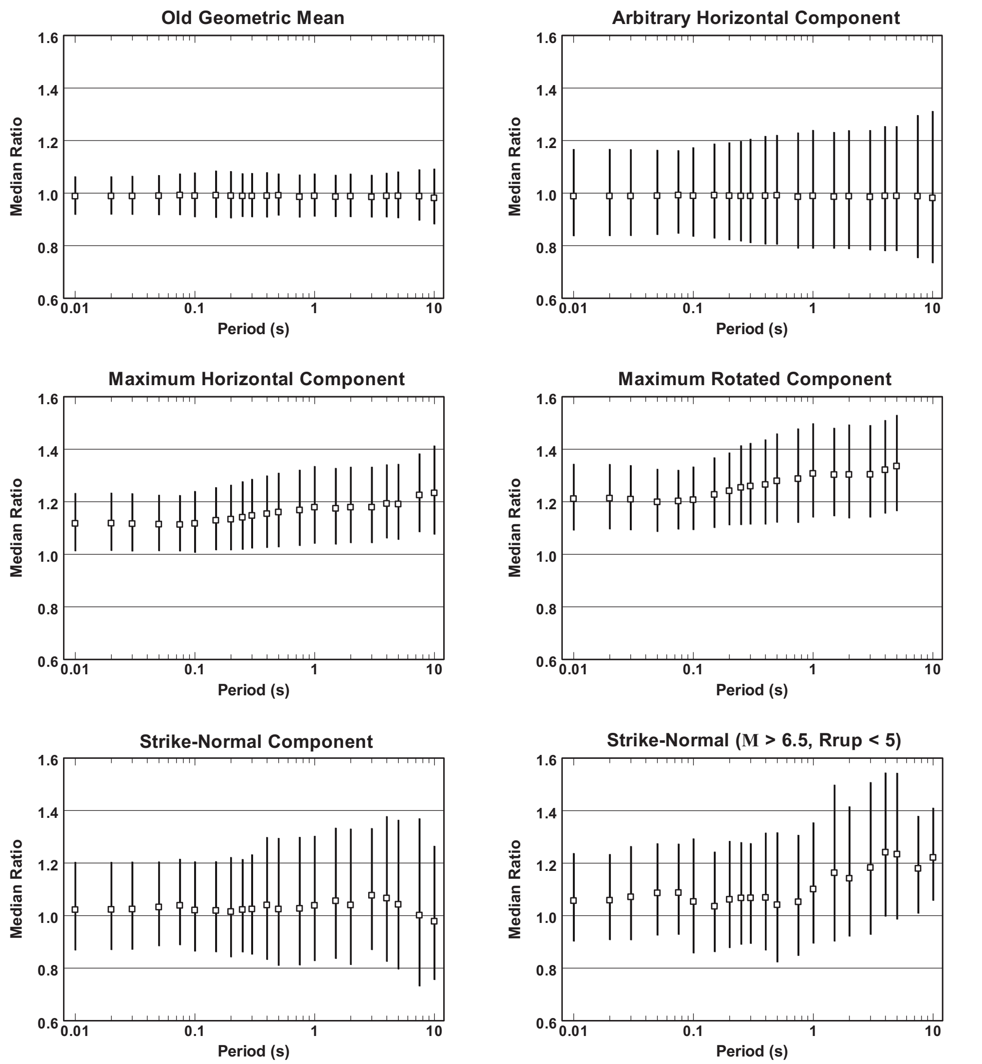

Figure 2. Estimated logarithmic ratios between selected alternative horizontal components and the new orientation-independent geometric mean horizontal component (GMRotI50). Vertical bars represent plus and minus one standard deviation in natural log units of an individual estimate of the logarithmic ratio. R_{RUP} has units of km.

$$f_{dis} = (c_4 + c_5\mathbf{M})\ln\left(\sqrt{R_{RUP}^2 + c_6^2}\right) \tag{3}$$

the style-of-faulting (fault mechanism) term is given by the expressions

$$f_{flt} = c_7 F_{RV} f_{flt,Z} + c_8 F_{NM} \tag{4}$$

$$f_{flt,Z} = \begin{cases} Z_{TOR}; & Z_{TOR} < 1 \\ 1; & Z_{TOR} \geq 1 \end{cases} \tag{5}$$

the hanging-wall term is given by the expressions

$$f_{hng} = c_9 f_{hng,R} f_{hng,M} f_{hng,Z} f_{hng,\delta} \tag{6}$$

$$f_{hng,R} = \begin{cases} 1; & R_{JB} = 0 \\ [\max(R_{RUP}, \sqrt{R_{JB}^2 + 1}) - R_{JB}]/\max(R_{RUP}, \sqrt{R_{JB}^2 + 1}); & R_{JB} > 0, Z_{TOR} < 1 \\ (R_{RUP} - R_{JB})/R_{RUP}; & R_{JB} > 0, Z_{TOR} \geq 1 \end{cases} \tag{7}$$

$$f_{hng,M} = \begin{cases} 0; & \mathbf{M} \leqslant 6.0 \\ 2(\mathbf{M} - 6.0); & 6.0 < \mathbf{M} < 6.5 \\ 1; & \mathbf{M} \geq 6.5 \end{cases} \tag{8}$$

$$f_{hng,Z} = \begin{cases} 0; & Z_{TOR} \geq 20 \\ (20 - Z_{TOR})/20; & 0 \leqslant Z_{TOR} < 20 \end{cases} \tag{9}$$

$$f_{hng,\delta} = \begin{cases} 1; & \delta \leqslant 70 \\ (90 - \delta)/20; & \delta > 70 \end{cases} \tag{10}$$

the shallow site response term is given by the expression

$$f_{site} = \begin{cases} c_{10} \ln\left(\dfrac{V_{S30}}{k_1}\right) + k_2 \left\{ \ln\left[A_{1100} + c\left(\dfrac{V_{S30}}{k_1}\right)^n\right] - \ln[A_{1100} + c] \right\}; & V_{S30} < k_1 \\ (c_{10} + k_2 n) \ln\left(\dfrac{V_{S30}}{k_1}\right); & k_1 \leqslant V_{S30} < 1100 \\ (c_{10} + k_2 n) \ln\left(\dfrac{1100}{k_1}\right); & V_{S30} \geq 1100 \end{cases} \tag{11}$$

the basin response term is given by the expression

$$f_{sed} = \begin{cases} c_{11}(Z_{2.5} - 1); & Z_{2.5} < 1 \\ 0; & 1 \leqslant Z_{2.5} \leqslant 3 \\ c_{12} k_3 e^{-0.75}[1 - e^{-0.25(Z_{2.5} - 3)}]; & Z_{2.5} > 3 \end{cases} \tag{12}$$

and $\hat{Y}$ is the median estimate of the geometric mean horizontal component (GMRotI50) of PGA (g), PGV (cm/s), PGD (cm) or PSA (g); $\mathbf{M}$ is moment magnitude; R_{RUP} is the closest distance to the coseismic rupture plane (km); R_{JB} is the closest distance to the surface projection of the coseismic rupture plane (km); F_{RV} is an indicator variable representing reverse and reverse-oblique faulting, where F_{RV}=1 for $30° < \lambda < 150°$, F_{RV} =0 otherwise, and λ is rake defined as the average angle of slip measured in the plane of rupture between the strike direction and the slip vector; F_{NM} is an indicator variable representing normal and normal-oblique faulting, where $F_{NM}=1$ for $-150° < \lambda < -30°$ and $F_{NM}=0$ otherwise; Z_{TOR} is the depth to the top of the coseismic rupture plane (km); δ is the dip of the rupture plane (°); V_{S30} is the time-averaged shear-wave velocity in the top 30 m of the site profile (m/s); A_{1100} is the median estimate of PGA on a reference rock outcrop ($V_{S30}=1100$ m/s) from Equation 11 (g); and $Z_{2.5}$ is the depth to the 2.5 km/s shear-wave velocity horizon, typically referred to as basin or sediment depth (km). The empirical coefficients c_i and the theoretical coefficients c, n and k_i are listed in Table 2. When PSA < PGA and $T \leq 0.25$ s, PSA should be set equal to PGA to be consistent with the definition of pseudo-absolute acceleration. This condition occurs only at large distances and small magnitudes.

ALEATORY UNCERTAINTY MODEL

Consistent with the random-effects regression analysis that was used to derive the median ground motion model, the aleatory uncertainty model is defined by the equation

$$\ln Y_{ij} = \ln \hat{Y}_{ij} + \eta_i + \varepsilon_{ij} \tag{13}$$

where η_i is the inter-event residual for event i; and $\hat{Y}_{ij}$, Y_{ij} and ε_{ij} are the predicted value, the observed value, and the intra-event residual for recording j of event i. The independent normally distributed variables η_i and ε_{ij} have zero means and estimated inter-event and intra-event standard deviations, τ and σ, given by

$$\tau = \tau_{\ln Y} \tag{14}$$

$$\sigma = \sqrt{\sigma^2_{\ln Y_B} + \sigma^2_{\ln AF} + \alpha^2 \sigma^2_{\ln A_B} + 2\alpha\rho\sigma_{\ln Y_B}\sigma_{\ln A_B}} \tag{15}$$

where the total standard deviation is

$$\sigma_T = \sqrt{\sigma^2 + \tau^2} \tag{16}$$

and $\tau_{\ln Y}$ is the standard deviation of the inter-event residuals; $\sigma_{\ln Y_B} = (\sigma^2_{\ln Y} - \sigma^2_{\ln AF})^{1/2}$ is the estimated standard deviation of ground motion at the base of the site profile; $\sigma_{\ln Y}$ is the standard deviation of the intra-event residuals; $\sigma_{\ln AF}$ is the estimated standard deviation of the logarithm of the site amplification factor (in this case f_{site}) assuming linear site response; $\sigma_{\ln A_B} = (\sigma^2_{\ln \mathrm{PGA}} - \sigma^2_{\ln AF})^{1/2}$ is the estimated standard deviation of PGA on reference rock at the base of the site profile; ρ is the correlation coefficient between the intra-event residuals of the ground motion parameter of interest and PGA; and α is the linearized functional relationship between f_{site} and $\ln A_{1100}$, which is estimated from the partial derivative (Abrahamson and Silva 2008, this volume):

Table 2. Coefficients for the geometric mean and arbitrary horizontal components of the median ground motion model

T (s)	c_0	c_1	c_2	c_3	c_4	c_5	c_6	c_7	c_8	c_9	c_{10}	c_{11}	c_{12}	k_1	k_2	k_3
0.010	−1.715	0.500	−0.530	−0.262	−2.118	0.170	5.60	0.280	−0.120	0.490	1.058	0.040	0.610	865	−1.186	1.839
0.020	−1.680	0.500	−0.530	−0.262	−2.123	0.170	5.60	0.280	−0.120	0.490	1.102	0.040	0.610	865	−1.219	1.840
0.030	−1.552	0.500	−0.530	−0.262	−2.145	0.170	5.60	0.280	−0.120	0.490	1.174	0.040	0.610	908	−1.273	1.841
0.050	−1.209	0.500	−0.530	−0.267	−2.199	0.170	5.74	0.280	−0.120	0.490	1.272	0.040	0.610	1054	−1.346	1.843
0.075	−0.657	0.500	−0.530	−0.302	−2.277	0.170	7.09	0.280	−0.120	0.490	1.438	0.040	0.610	1086	−1.471	1.845
0.10	−0.314	0.500	−0.530	−0.324	−2.318	0.170	8.05	0.280	−0.099	0.490	1.604	0.040	0.610	1032	−1.624	1.847
0.15	−0.133	0.500	−0.530	−0.339	−2.309	0.170	8.79	0.280	−0.048	0.490	1.928	0.040	0.610	878	−1.931	1.852
0.20	−0.486	0.500	−0.446	−0.398	−2.220	0.170	7.60	0.280	−0.012	0.490	2.194	0.040	0.610	748	−2.188	1.856
0.25	−0.890	0.500	−0.362	−0.458	−2.146	0.170	6.58	0.280	0.000	0.490	2.351	0.040	0.700	654	−2.381	1.861
0.30	−1.171	0.500	−0.294	−0.511	−2.095	0.170	6.04	0.280	0.000	0.490	2.460	0.040	0.750	587	−2.518	1.865
0.40	−1.466	0.500	−0.186	−0.592	−2.066	0.170	5.30	0.280	0.000	0.490	2.587	0.040	0.850	503	−2.657	1.874
0.50	−2.569	0.656	−0.304	−0.536	−2.041	0.170	4.73	0.280	0.000	0.490	2.544	0.040	0.883	457	−2.669	1.883
0.75	−4.844	0.972	−0.578	−0.406	−2.000	0.170	4.00	0.280	0.000	0.490	2.133	0.077	1.000	410	−2.401	1.906
1.0	−6.406	1.196	−0.772	−0.314	−2.000	0.170	4.00	0.255	0.000	0.490	1.571	0.150	1.000	400	−1.955	1.929
1.5	−8.692	1.513	−1.046	−0.185	−2.000	0.170	4.00	0.161	0.000	0.490	0.406	0.253	1.000	400	−1.025	1.974
2.0	−9.701	1.600	−0.978	−0.236	−2.000	0.170	4.00	0.094	0.000	0.371	−0.456	0.300	1.000	400	−0.299	2.019
3.0	−10.556	1.600	−0.638	−0.491	−2.000	0.170	4.00	0.000	0.000	0.154	−0.820	0.300	1.000	400	0.000	2.110
4.0	−11.212	1.600	−0.316	−0.770	−2.000	0.170	4.00	0.000	0.000	0.000	−0.820	0.300	1.000	400	0.000	2.200
5.0	−11.684	1.600	−0.070	−0.986	−2.000	0.170	4.00	0.000	0.000	0.000	−0.820	0.300	1.000	400	0.000	2.291
7.5	−12.505	1.600	−0.070	−0.656	−2.000	0.170	4.00	0.000	0.000	0.000	−0.820	0.300	1.000	400	0.000	2.517
10.0	−13.087	1.600	−0.070	−0.422	−2.000	0.170	4.00	0.000	0.000	0.000	−0.820	0.300	1.000	400	0.000	2.744
PGA	−1.715	0.500	−0.530	−0.262	−2.118	0.170	5.60	0.280	−0.120	0.490	1.058	0.040	0.610	865	−1.186	1.839
PGV	0.954	0.696	−0.309	−0.019	−2.016	0.170	4.00	0.245	0.000	0.358	1.694	0.092	1.000	400	−1.955	1.929
PGD	−5.270	1.600	−0.070	0.000	−2.000	0.170	4.00	0.000	0.000	0.000	−0.820	0.300	1.000	400	0.000	2.744

Note: c=1.88 and n=1.18 for all periods (T); PGA and PSA have units of g; PGV and PGD have units of cm/s and cm, respectively.

Table 3. Standard deviations and correlation coefficients for the aleatory uncertainty model

	Standard Deviation for $V_{S30} \geq k_1$					Correlation Coefficient
T (s)	$\sigma_{\ln Y}$	$\tau_{\ln Y}$	σ_C	σ_T	σ_{Arb}	ρ
0.010	0.478	0.219	0.166	0.526	0.551	1.000
0.020	0.480	0.219	0.166	0.528	0.553	0.999
0.030	0.489	0.235	0.165	0.543	0.567	0.989
0.050	0.510	0.258	0.162	0.572	0.594	0.963
0.075	0.520	0.292	0.158	0.596	0.617	0.922
0.10	0.531	0.286	0.170	0.603	0.627	0.898
0.15	0.532	0.280	0.180	0.601	0.628	0.890
0.20	0.534	0.249	0.186	0.589	0.618	0.871
0.25	0.534	0.240	0.191	0.585	0.616	0.852
0.30	0.544	0.215	0.198	0.585	0.618	0.831
0.40	0.541	0.217	0.206	0.583	0.618	0.785
0.50	0.550	0.214	0.208	0.590	0.626	0.735
0.75	0.568	0.227	0.221	0.612	0.650	0.628
1.0	0.568	0.255	0.225	0.623	0.662	0.534
1.5	0.564	0.296	0.222	0.637	0.675	0.411
2.0	0.571	0.296	0.226	0.643	0.682	0.331
3.0	0.558	0.326	0.229	0.646	0.686	0.289
4.0	0.576	0.297	0.237	0.648	0.690	0.261
5.0	0.601	0.359	0.237	0.700	0.739	0.200
7.5	0.628	0.428	0.271	0.760	0.807	0.174
10.0	0.667	0.485	0.290	0.825	0.874	0.174
PGA	0.478	0.219	0.166	0.526	0.551	1.000
PGV	0.484	0.203	0.190	0.525	0.558	0.691
PGD	0.667	0.485	0.290	0.825	0.874	0.174

Note: see text for the calculation of standard deviations for $V_{S30} < k_1$.

$$\alpha = \frac{\partial f_{site}}{\partial \ln A_{1100}} = \begin{cases} k_2 A_{1100}\{[A_{1100} + c(V_{S30}/k_1)^n]^{-1} - (A_{1100} + c)^{-1}\} & V_{S30} < k_1 \\ 0 & V_{S30} \geqslant k_1 \end{cases} \tag{17}$$

The coefficients k_1, k_2, c and n are listed in Table 2. The standard deviations $\tau_{\ln Y}$, $\sigma_{\ln Y}$, $\sigma_{\ln \mathrm{PGA}}$, and $\sigma_{\ln AF}$ and the correlation coefficient ρ are listed in Table 3. The value of ρ at long periods was constrained to be a constant consistent with its statistical variability with period.

Equation 14 recognizes that τ is approximately equal to the standard deviation of the inter-event residuals, $\tau_{\ln Y}$, which is consistent with the common understanding that inter-event terms are not significantly affected by soil nonlinearity (e.g., Kwok and Stewart 2006; J. Stewart, personal communication 2007). Even if we were to assume that

τ was subject to soil nonlinearity effects (e.g., Abrahamson and Silva 2008, this volume), it would have only a relatively small effect on the total standard deviation because of the dominance of the intra-event standard deviation in Equation 16. The more complicated relationship for σ takes into account the soil nonlinearity effects embodied in Equation 11, which predicts that as the value of A_{1100} increases the corresponding value of f_{site} decreases for soils in which $V_{S30} < k_1$ (i.e., soft soils). This nonlinearity impacts the intra-event standard deviation by reducing the variability in the site amplification factor at high values of A_{1100} as modeled by the first-order second-moment approximation of σ given in Equation 15. This approximation was first introduced by Bazzurro and Cornell (2004b) for the case in which PSA is used as the reference rock ground motion and later extended by Stewart and Goulet (2006) to our case in which PGA is used as the reference rock ground motion.

The development of the aleatory uncertainty model presented above assumes that $\sigma_{\ln Y}$ and $\sigma_{\ln \mathrm{PGA}}$ represent the aleatory uncertainty associated with linear site response. This assumption reflects the dominance of such recordings in our database. Another key element in this formulation is the selection of an appropriate value for $\sigma_{\ln AF}$. Although this value can be impacted by many factors, site response studies using both empirical methods (e.g., Baturay and Stewart 2003) and theoretical methods (e.g., Silva et al. 1999, 2000; Bazzurro and Cornell 2004a, 2005) suggest that a period-independent value of $\sigma_{\ln AF} \approx 0.3$ is a reasonable value for deep soil sites (at least once 3-D basin response has been removed as in the case of our model). This uncertainty is expected to decrease as sites become harder (Silva et al. 1999, 2000), but since such sites do not respond nonlinearly, σ is not sensitive to the value of $\sigma_{\ln AF}$.

Baturay and Stewart (2003), Stewart et al. (2003), and Choi and Stewart (2005) also found the intra-event standard deviation to be dependent on site classification and V_{S30} at short periods. They found that softer sites had a lower standard deviation than harder sites, presumably as a result of nonlinear site response (e.g., Bazzurro and Cornell 2004b). Since we include the effects of soil nonlinearity in our model (Figure 6), we were able to test this hypothesis by binning our intra-event residuals for PGA and PSA at periods of 0.2, 1 and 3 s into V_{S30} ranges representing NEHRP site classes C ($V_{S30} = 360-760$ m/s) and D ($V_{S30} = 180-360$ m/s) and performing a hypothesis test to see if the differences in the mean residuals of these two site classes were statistically significant. We found that the mean residuals for each of the velocity bins were not significantly different from zero (i.e., they were unbiased) at the 95% confidence level and that the residual standard deviations of the two bins differed by less than 6%. Based on these results, we concluded that the intra-event standard deviation for our model is not dependent on V_{S30} once nonlinear site effects are taken into account.

As discussed previously, in some applications engineers require an estimate of the aleatory uncertainty of the arbitrary horizontal component (Baker and Cornell 2006). In such cases, the following equation can be used to calculate this standard deviation:

$$\sigma_{Arb} = \sqrt{\sigma_T^2 + \sigma_C^2} \tag{18}$$

where σ_C is given by the equation (Boore 2005)

$$\sigma_C^2 = \frac{1}{4N}\sum_{j=1}^{N} (\ln y_{1j} - \ln y_{2j})^2 \qquad (19)$$

and y_{ij} is the value of the ground motion parameter for component i of recording j and N is the total number of recordings. Strictly speaking, the value of σ_C estimated in this manner is calculated with respect to the orientation-dependent (old) version of the geometric mean and not the orientation-independent (new) version of the geometric mean used in this study. However, the difference is negligible considering the similarity in the two horizontal geometric mean components (Beyer and Bommer 2006; Boore et al. 2006; Campbell and Bozorgnia 2007). Values of σ_C calculated from Equation 19 are listed in Table 3. Also listed in this table for reference are the values of σ_T and σ_{Arb} for ground motions subject to linear site response (i.e., for $V_{S30} \geq k_1$ or small values of A_{1100}).

MODEL EVALUATION

An evaluation of our NGA ground motion model is presented in Figures 3–9. Figures 3–5 show the scaling of the median estimates of PGA, PGV and PSA at periods of 0.2, 1, 3 and 10 s with rupture distance, moment magnitude, style of faulting, and hanging-wall effects. Figure 6 shows the dependence of the total standard deviation on rock PGA. Figures 7–9 show the scaling of the median estimate of PSA with magnitude, 30-m shear-wave velocity, and basin depth. Figure 9 also shows a plot of the basin response term. Campbell and Bozorgnia (2007) present many additional plots as well as a table of predicted values that can be used to verify a user's implementation of the model. A spreadsheet and computer code are also available from the authors upon request.

DISCUSSION OF FUNCTIONAL FORMS

This section presents a discussion of the functional forms that we used to define the various mathematical terms in the median ground motion and aleatory uncertainty models. We present several plots that show the dependence of model residuals on magnitude and distance to confirm the general validity of the models. Similar plots for other explanatory variables, including those that were evaluated but not included in the model, are given in Campbell and Bozorgnia (2007). Residual plots are shown for PGA, PGV and PSA at periods of 0.2, 1, 3 and 10 s. A positive residual indicates underestimation by the model; whereas, a negative residual indicates overestimation by the model. The discussion of the functional forms is followed by a brief discussion of the constraints that we applied to our model in order to extend it to long periods. Further justification of the functional forms and related constraints is given in Campbell and Bozorgnia (2007).

MAGNITUDE TERM

We used an analysis of residuals to derive the trilinear functional form for f_{mag}. This functional form was used to model magnitude saturation effects at short distances that were recognized and modeled by Campbell (1981) over 25 years ago. The piecewise linear relationship allows greater control of large-magnitude ($\mathbf{M} > 6.5$) scaling and, unlike the more commonly used quadratic relationship, decouples this scaling from that of

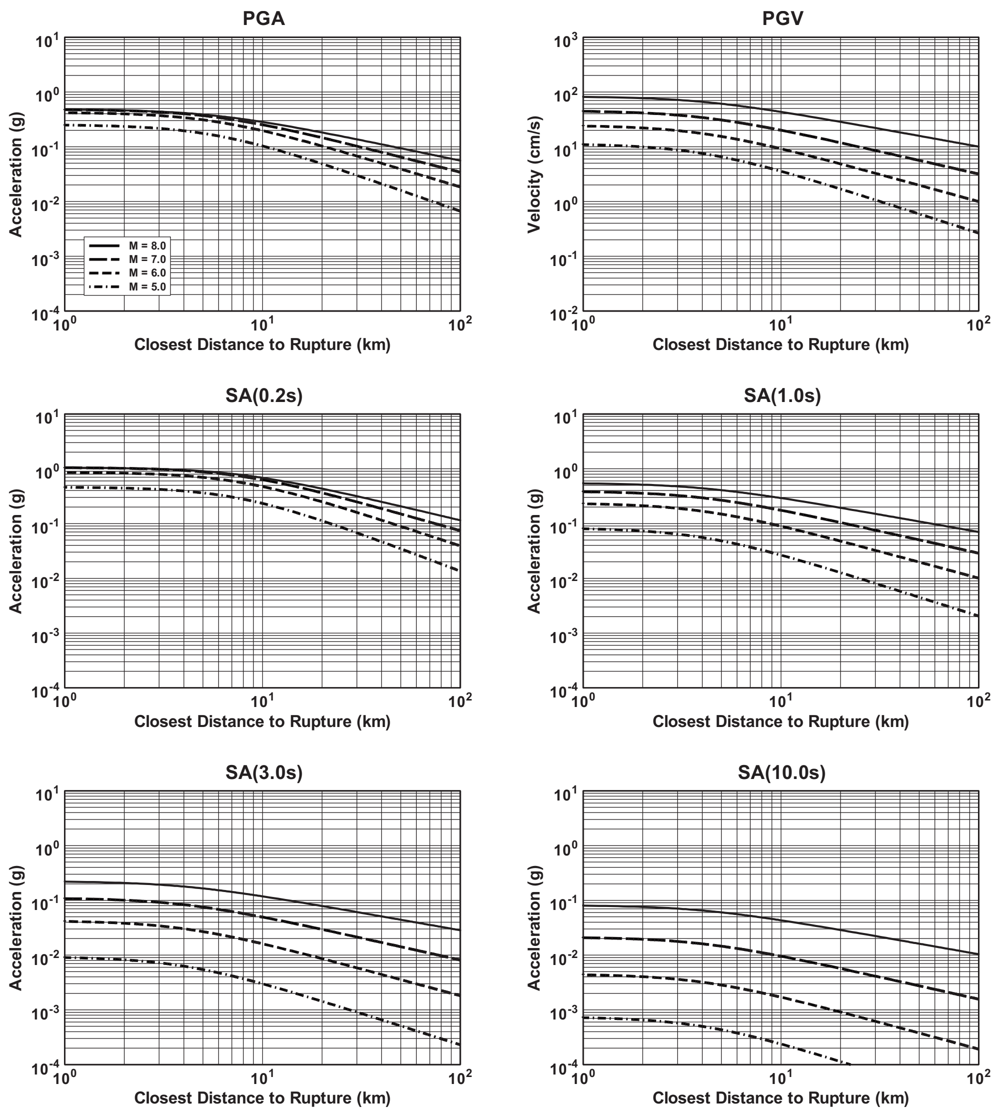

Figure 3. Predicted attenuation of ground motion with rupture distance (R_{RUP}) showing its dependence on moment magnitude (**M**). The ground motion model is evaluated for $\mathbf{M}$=5.0, 6.0, 7.0 and 8.0; F_{RV}=F_{NM}=0; V_{S30}=760 m/s; and $Z_{2.5}$=2 km.

smaller magnitudes allowing more flexibility in determining how ground motions scale with earthquake size. Stochastic simulations conducted by the authors demonstrated that the trilinear model was able to fit the magnitude scaling characteristics of ground motion just as well as the quadratic model for $\mathbf{M} \leq 6.5$, where magnitude saturation is not an issue. The large-magnitude scaling predicted by the trilinear model was also found to be consistent with the observed effects of aspect ratio (i.e., rupture length divided by rup-

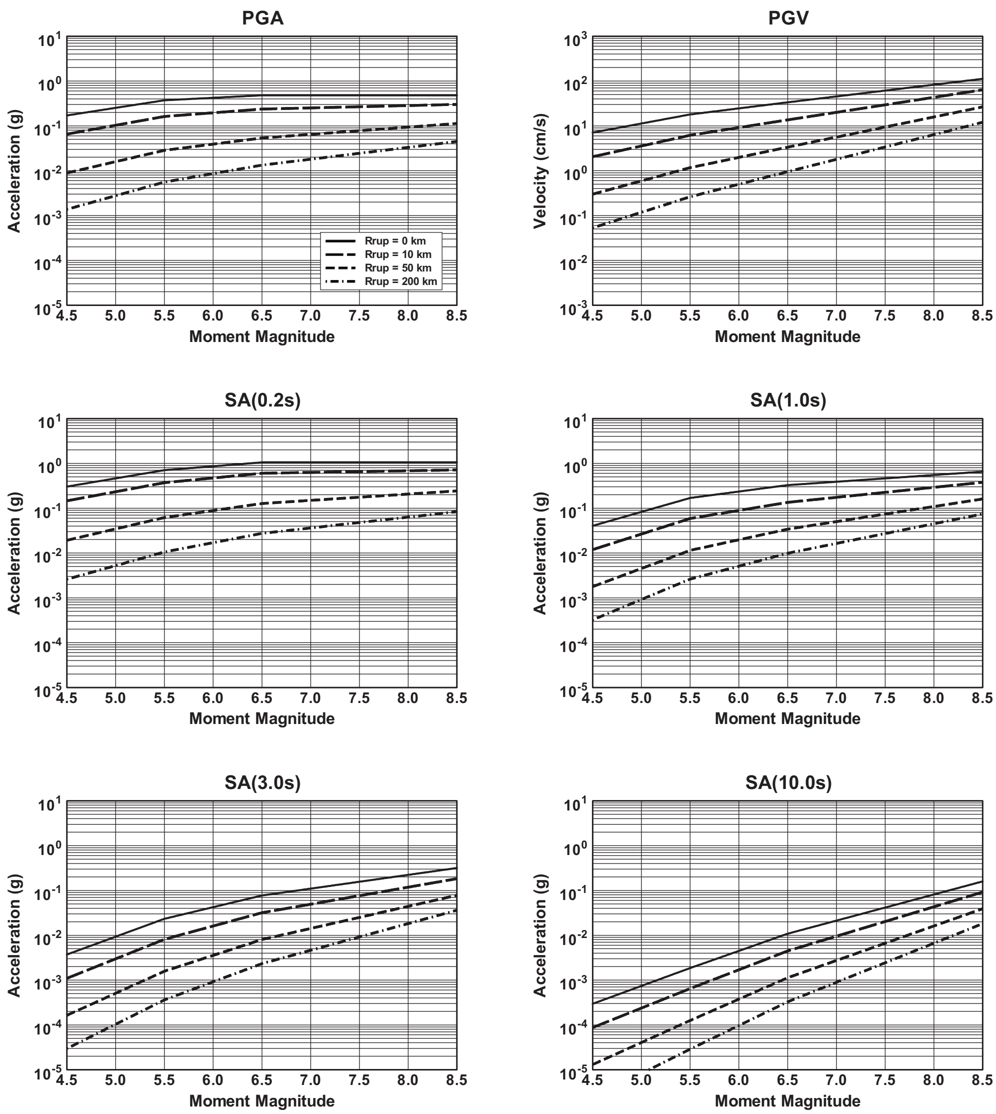

Figure 4. Predicted scaling of ground motion with moment magnitude (**M**) showing its dependence on rupture distance (R_{RUP}). The ground motion model is evaluated for R_{RUP}=0, 10, 50 and 200 km; F_{RV}=F_{NM}=0; V_{S30}=760 m/s; and $Z_{2.5}$=2 km.

ture width), which we chose to abandon as an explanatory variable when we found an inconsistency between the aspect ratios in the PEER NGA database and those predicted by published rupture dimension versus magnitude relationships (Campbell and Bozorgnia 2007).

The original unconstrained regression analyses resulted in the prediction of oversatu-

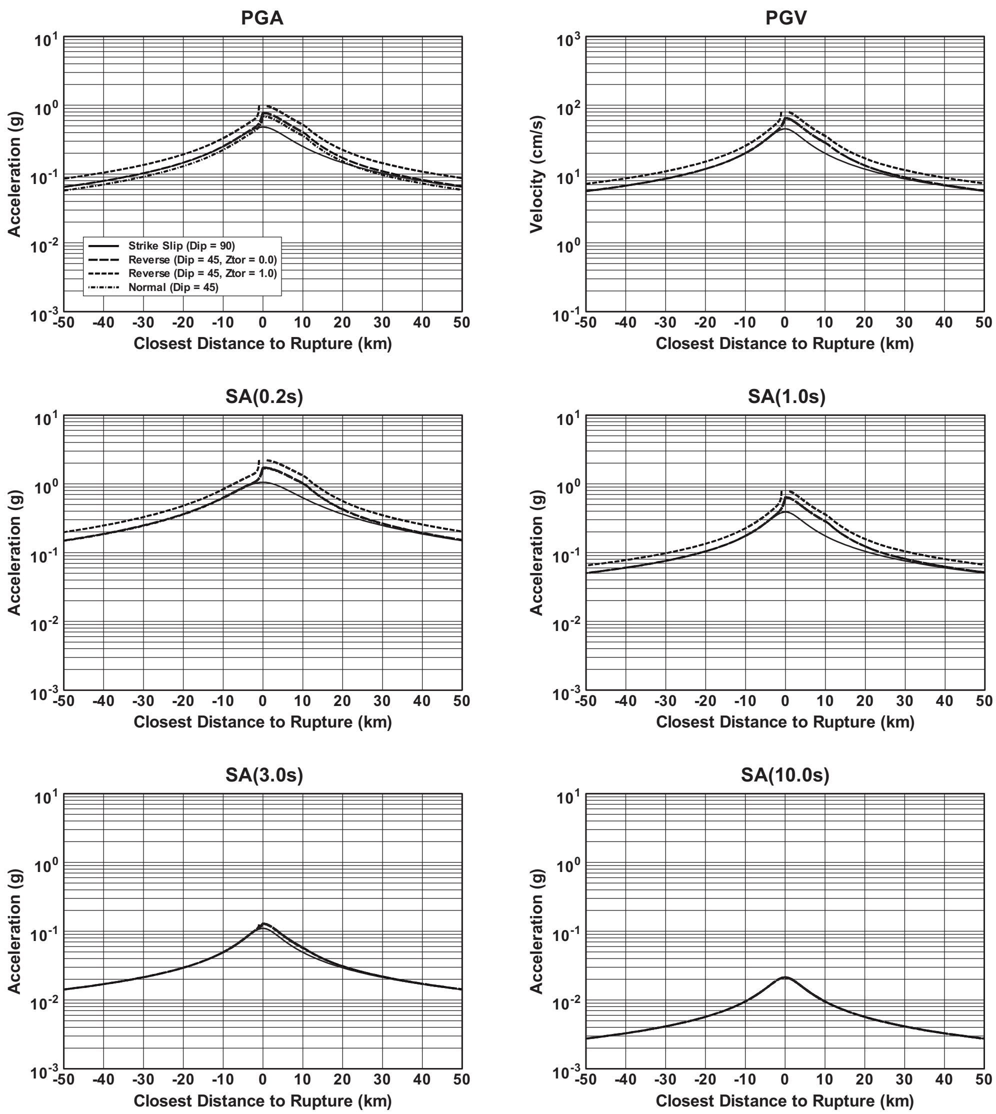

Figure 5. Predicted attenuation of ground motion with rupture distance (R_{RUP}) showing its dependence on style of faulting. The ground motion model is evaluated for strike-slip ($F_{RV}=F_{NM}=0$), surface-reverse ($F_{RV}=1$, $F_{NM}=0$, $Z_{TOR}=0$), buried-reverse ($F_{RV}=1$, $F_{NM}=0$, $Z_{TOR}=1$ km), and normal ($F_{RV}=0$, $F_{NM}=1$) faulting; $\mathbf{M}=7.0$; $V_{S30}=760$ m/s; and $Z_{2.5}=2$ km. For dip-slip faults, the rupture plane dips 45° from $R_{RUP}=0$ to $R_{RUP}=10$ km. Negative distances correspond to sites on the footwall and positive distances to sites on the hanging wall.

ration (amplitudes that decrease with magnitude) at short periods for large magnitudes and short distances. This behavior, which had been noted in previous studies but not found to be statistically significant, was reinforced in this study by the addition of some recent well-recorded large-magnitude earthquakes (Table 1). Although some seismolo-

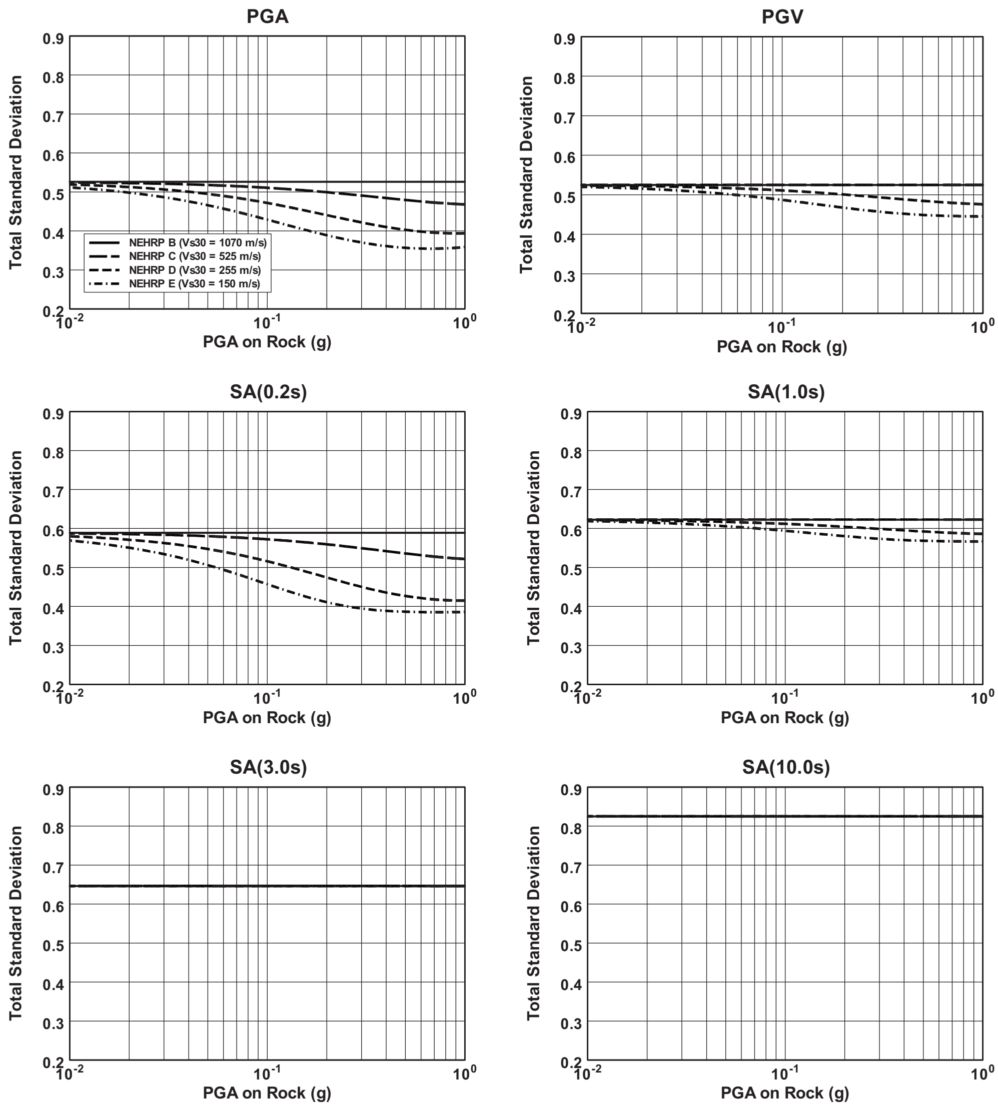

Figure 6. Predicted dependence of the total standard deviation (σ_T) of the natural logarithm of the geometric mean ground motion with rock PGA (A_{1100}) showing its dependence on 30-m shear-wave velocity (V_{S30}). The aleatory uncertainty model is evaluated for V_{S30}=1070 m/s (NEHRP B), V_{S30}=525 m/s (NEHRP C), V_{S30}=255 m/s (NEHRP D) and V_{S30}=150 m/s (NEHRP E).

gists believe that such a reduction in short-period ground motion is possible for very large earthquakes (e.g., Schmedes and Archuleta 2007), this behavior was not found to be statistically significant in our study even after including the additional supporting data. Considering this weak statistical evidence and the lack of scientific consensus in

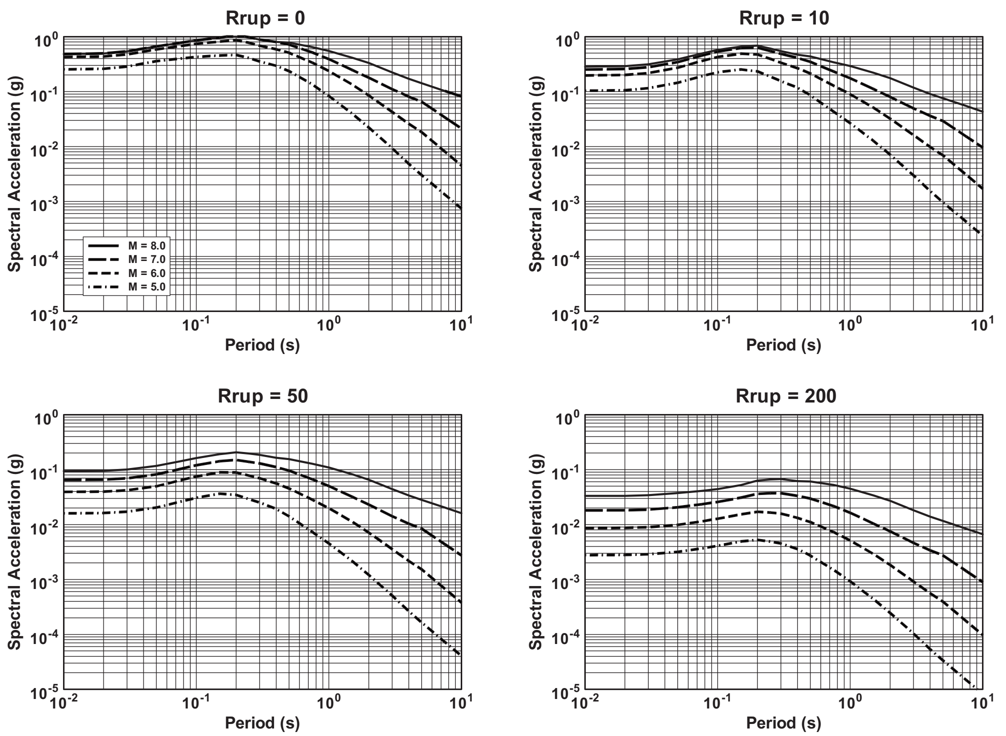

Figure 7. Predicted dependence of 5% damped pseudo-acceleration response spectra on moment magnitude (**M**) and rupture distance (R_{RUP}). The ground motion model is evaluated for $\mathbf{M}$=5.0, 6.0, 7.0 and 8.0; R_{RUP}=0, 10, 50 and 200 km; $F_{RV}=F_{NM}=0$; V_{S30}=760 m/s; and $Z_{2.5}$=2 km.

support of oversaturation, we conservatively constrained f_{mag} to saturate at $\mathbf{M}>6.5$ and $R_{RUP}=0$ when oversaturation was predicted by the unconstrained regression analysis. This constraint was equivalent to setting $c_3=-c_1-c_2-c_5\ln(c_6)$ in Equation 2. Figures 10 and 11 show the dependence of the inter-event and intra-event residuals on moment magnitude after applying the saturation constraint. These plots confirm that the ground motion estimates from our NGA model are relatively unbiased with respect to magnitude, except at larger magnitudes where the saturation constraint leads to an overestimation of short-period ground motion.

If we isolate events recorded in a specific region, we can observe an apparent bias in their inter-event residuals with respect to the population as a whole. An example is the generally positive inter-event residuals at relatively long periods of large-magnitude ($\mathbf{M}>6.7$) earthquakes in California. However, in the example for California, the apparent bias is based on only five events (one of which has only one recording) and, in our opinion, is not sufficient to define the magnitude scaling characteristics of large-magnitude earthquakes in this region. Nonetheless, if the user wants to take such a bias

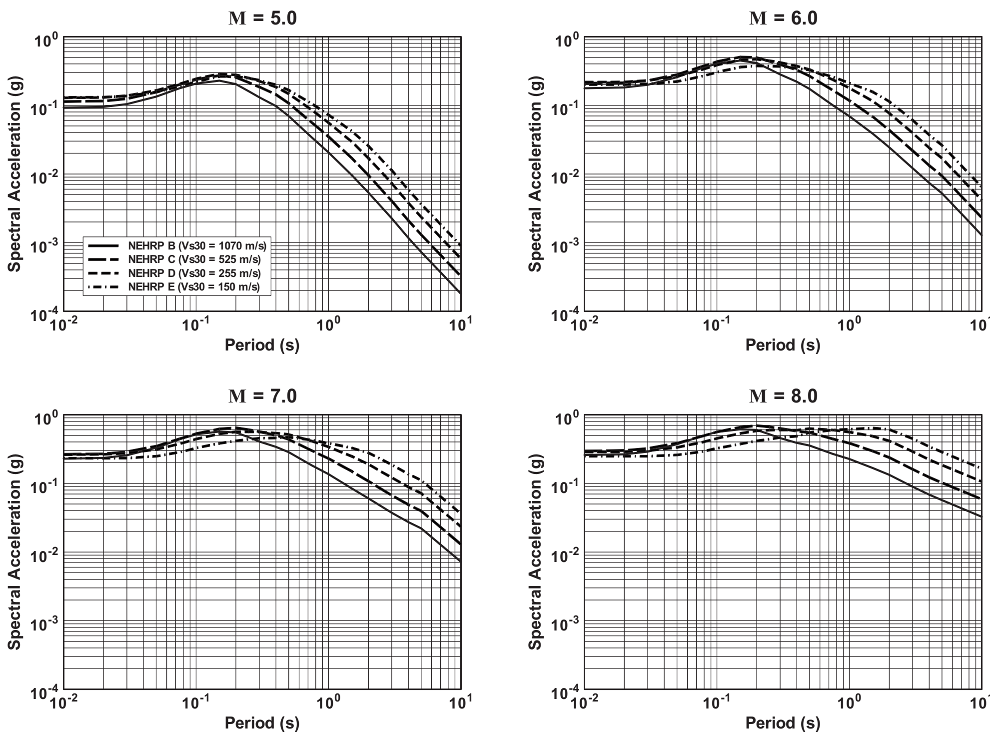

Figure 8. Predicted dependence of 5% damped pseudo-acceleration response spectra on 30-m shear-wave velocity (V_{S30}). The ground motion model is evaluated for V_{S30}=1070 m/s (NEHRP B), V_{S30}=525 m/s (NEHRP C), V_{S30}=255 m/s (NEHRP D) and V_{S30}=150 m/s (NEHRP E); **M**=5.0, 6.0, 7.0 and 8.0; $F_{RV}=F_{NM}=0$; R_{RUP}=10 km; and $Z_{2.5}$=2 km.

into account, whether statistically significant or not, this can be accomplished by increasing the level of conservatism in the ground motion estimates by, for example, including additional epistemic uncertainty.

DISTANCE TERM

Our previous model (Campbell and Bozorgnia 2003), which was developed for distances of 60 km and less, had a constant rate of attenuation independent of magnitude. In order to extend our ground motion model to distances of 200 km, we found it necessary to include a magnitude-dependent slope in the distance term given by Equation 3 (e.g., Abrahamson and Silva 1997). A computational advantage of this functional form is that it transfers the magnitude-dependent attenuation term from inside the square-root, as in our previous model, to outside the square-root, significantly improving the stability of the nonlinear regression analysis. Frankel (2007) used broadband ground motion simulations of extended fault sources to show that the theoretical attenuation of response spectral ordinates was consistent with our functional form for magnitudes of 6.5 and 7.5 and distances of 2–100 km. Our distance term was also found to meet the simple the-

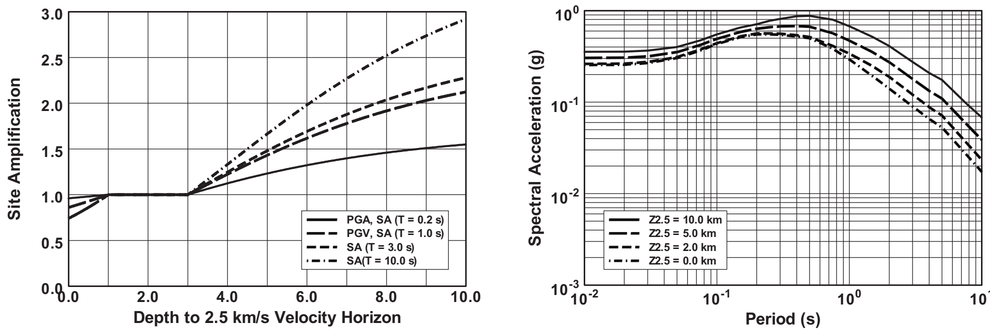

Figure 9. Predicted basin effects of PGA, PGV and 5% damped pseudo-acceleration response spectra: (left) predicted scaling of the basin response term with basin depth ($Z_{2.5}$); (right) predicted dependence of 5% damped pseudo-acceleration response spectra on basin depth. The ground motion model is evaluated for $Z_{2.5}$=0, 5, 2 and 10 km; **M**=7.0; F_{RV}=F_{NM}=0; R_{RUP} =10 km; and V_{S30}=760 m/s.

oretical constraints provided to the NGA project by Jack Boatwright (written communication, 2006; see also Campbell and Bozorgnia 2007). Figure 12 shows the dependence of the intra-event residuals on rupture distance. This plot confirms that the ground motion estimates from our NGA model are relatively unbiased with respect to distance.

STYLE-OF-FAULTING TERM

The functional form used to model f_{flt} was determined from an analysis of residuals. It introduces a new parameter, Z_{TOR}, that represents whether or not coseismic rupture extends to the surface. This new parameter was found to be important for modeling reverse-faulting events. We found that ground motions were significantly higher for reverse-faulting events when rupture did not propagate to the surface, regardless of whether this rupture was on a blind thrust fault or on a fault with previous surface rupture. When rupture broke to the surface or to very shallow depths, ground motions for reverse-faulting events were found to be comparable on average to those for strike-slip events. Some strike-slip ruptures with partial or weak surface expression also appeared to have higher-than-average ground motion, but other strike-slip events appeared to contradict this observation. Some of these discrepancies could be due to the ambiguity in identifying coseismic surface rupture for many strike-slip events in the PEER NGA database. As a result, we decided that additional study would be needed to resolve these discrepancies before it was possible to reliably include Z_{TOR} as an explanatory variable for strike-slip events.

The model coefficient for normal faulting was found to be only marginally significant at short periods but very significant at long periods. We believe that the observed long-period effects are due to systematic differences in sediment depth rather than to any inherent source effect. Many of these events occurred in a geological and tectonic environment that might be associated with shallow depths to hard rock (e.g., events in Italy,

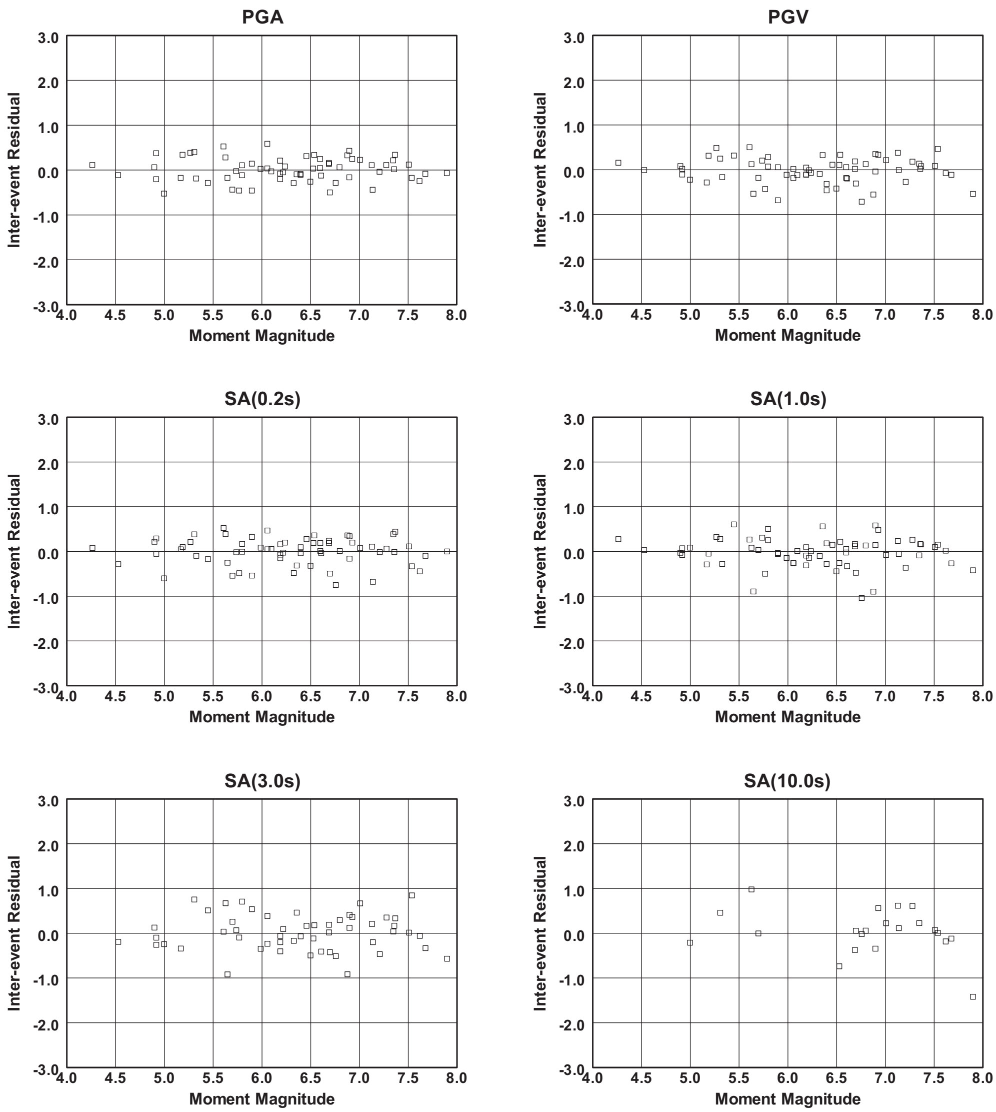

Figure 10. Dependence of inter-event residuals on moment magnitude (**M**).

Greece, and the United States Basin and Range province), but because there were no estimates of sediment depth for these recording sites in the PEER NGA database, they could not be corrected for potential depth effects in the regression analyses. This hypothesis is corroborated by Ambraseys et al. (2005) and Akkar and Bommer (2007), who found that strike-slip and normal-faulting ground motions from tectonically active regions in Europe and the Middle East had similar spectral amplitudes at moderate-to-long periods and somewhat smaller spectral amplitudes at short periods. As a result, we

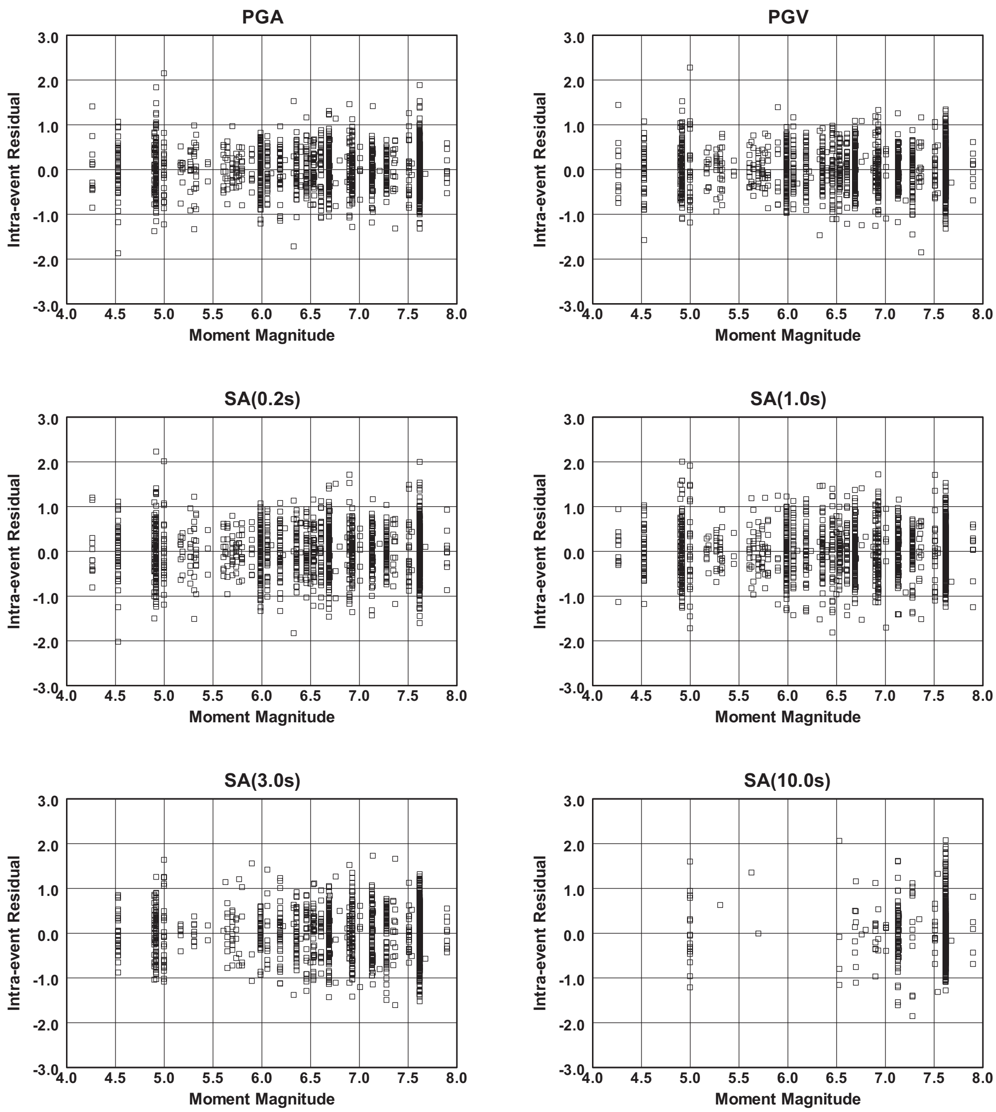

Figure 11. Dependence of intra-event residuals on moment magnitude (**M**).

constrained the relatively small normal-faulting factor (F_{NM}) found at short periods, a reduction of around 12%, to go to zero at long periods to be consistent with the findings of these investigators.

HANGING-WALL TERM

The functional form used to model f_{hng} was determined from an analysis of residuals with additional constraints to limit its range of applicability. The functional form used to model $f_{hng,R}$ (Campbell and Bozorgnia 2007; modified from Chiou and Youngs 2008, this volume) constrains the hanging-wall factor to have a smooth transition between the

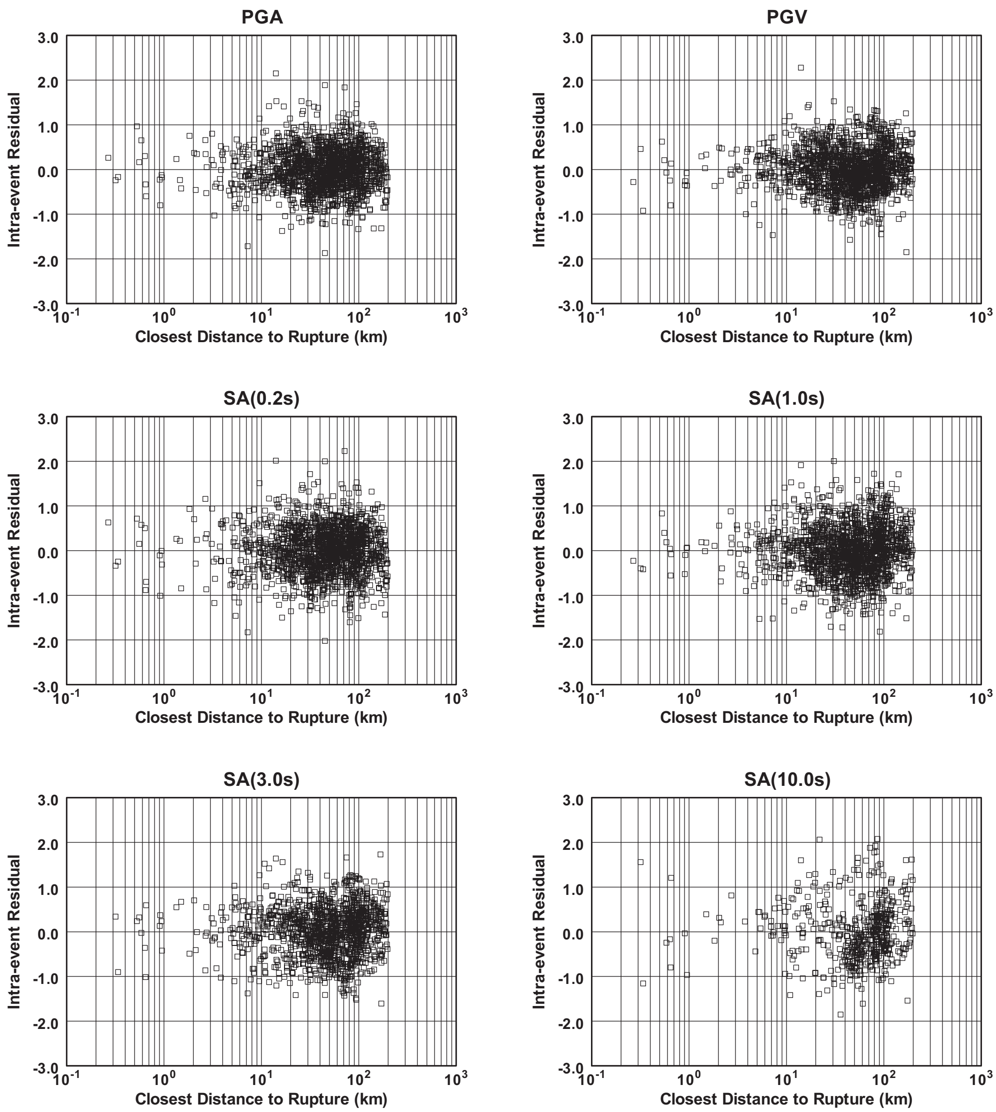

Figure 12. Dependence of intra-event residuals on rupture distance (R_{RUP}).

hanging wall and the footwall, even at small values of Z_{TOR}, which avoids an abrupt drop in the predicted value of ground motion for sites located directly across the fault trace from one another. We also included the additional functions $f_{hng,M}$, $f_{hng,Z}$ and $f_{hng,\delta}$ to phase out hanging-wall effects at small magnitudes, large rupture depths, and large rupture dips, where the residuals suggested that these effects are either negligible or irresolvable from the data.

Unlike our previous model (Campbell and Bozorgnia 2003), we have included hanging-wall effects for normal-faulting and non-vertical strike-slip earthquakes in our NGA model. Although the statistical evidence for hanging-wall effects for normal faulting is weak, we found that the hanging-wall factor was consistent with the better-constrained hanging-wall factor found for reverse faults. Furthermore, Jim Brune (personal communication, 2006) has found that normal faults exhibit hanging-wall effects from laboratory experiments of simulated fault rupture in foam rubber. He also found that his foam-rubber modeling results were consistent with the limited amount of precarious rock observations on the hanging wall of normal faults with documented historical and Holocene rupture in the Basin and Range. In a study on broadband simulations of ground motion in the Basin and Range, Collins et al. (2006) found the hanging-wall factor for normal-faulting events to be similar to the one we found empirically for reverse-faulting events. It should be noted that, unlike a reverse fault, the hanging wall of a normal fault will typically lie beneath the range front valley, where the majority of the population and infrastructure is likely to be located (e.g., Reno, Nevada and Salt Lake City, Utah).

SHALLOW SITE RESPONSE TERM

The linear part of the functional form used to model f_{site} is similar to that proposed by Borcherdt (1994) and Boore et al. (1997), except that we hold the site term constant for $V_{S30} > 1100$ m/s. This constraint was imposed after an analysis of residuals indicated that ground motions at long periods and high values of V_{S30} were underestimated by the model when this constraint was not applied. This velocity constraint should have probably been applied at even a smaller value of V_{S30} at long periods, but that would have complicated the use of the nonlinear site term. Since there are only a limited number of recordings with $V_{S30} > 1100$ m/s in our database, we believe that a more refined velocity constraint is unwarranted at this time.

After including the linear part of the shallow site response term in the model, we found that the residuals clearly exhibited a bias when plotted against rock PGA, A_{1100}, consistent with the nonlinear behavior of PGA and PSA at short periods. However, because of the relatively small number of recordings, the residuals alone were not sufficient to determine how this behavior varied with V_{S30}, ground motion amplitude, and oscillator period. Choi and Stewart (2005) empirically modeled this behavior using a linear relationship between the logarithms of site amplification and rock PGA with a slope that was a piecewise linear function of V_{S30}. In order to allow an extrapolation of this linear function to smaller and larger values of A_{1100}, we used a more complex nonlinear site response term that was developed by Walling et al. (2008, this volume), from 1-D equivalent-linear site response simulations sponsored by the NGA project (Power et al. 2008, this volume) in order to constrain the functional form and the nonlinear model coefficients k_1, k_2, n and c in Equation 11. This approach is supported by Kwok and Stewart (2006), who found that theoretical site factors from 1-D equivalent-linear site response analyses were able to capture the average effects of soil nonlinearity when used in conjunction with empirical ground motion models. Figure 13 shows the dependence of f_{site} on rock PGA that is predicted by our model.

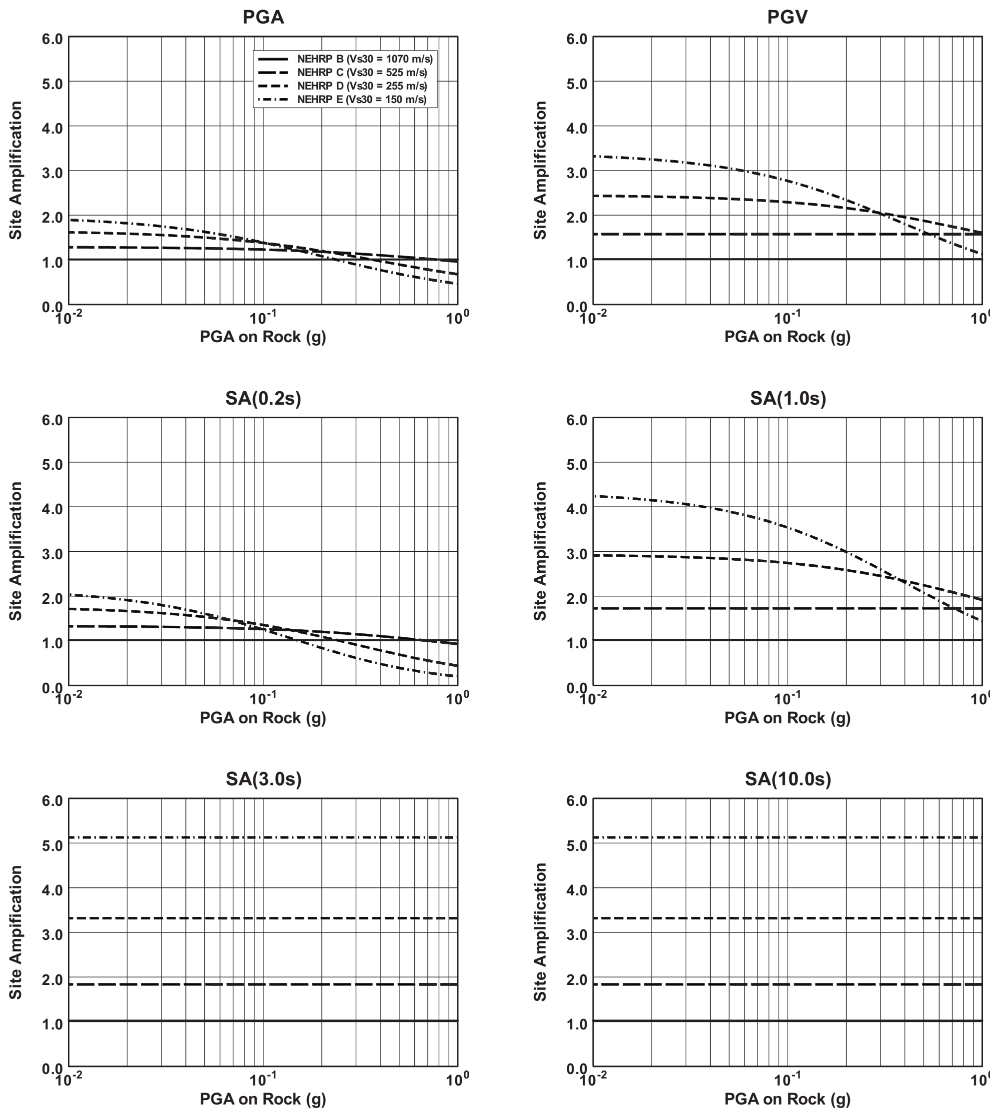

Figure 13. Predicted dependence of shallow site amplification on rock PGA (A_{1100}) showing its dependence on 30-m shear-wave velocity (V_{S30}). The site amplification is evaluated for V_{S30} =1070 m/s (NEHRP B), V_{S30}=525 m/s (NEHRP C), V_{S30}=255 m/s (NEHRP D) and V_{S30} =150 m/s (NEHRP E).

BASIN RESPONSE TERM

The function f_{sed} is composed of two parts: (1) a term to model 3-D basin response for $Z_{2.5} > 3$ km and (2) a term to model shallow sediment effects for $Z_{2.5} < 1$ km. We modeled the basin term from theoretical studies conducted as part of the NGA project (Day et al. 2008, this volume; Power et al. 2008, this volume). We empirically modeled the shallow sediment term based on an analysis of residuals. The model residuals after including the shallow site response term, f_{site}, clearly indicated that the amplitude of long-period ground motion increased with sediment depth up to around $Z_{2.5}=1$ km, leveled off, then increased again at $Z_{2.5}>3$ km. We surmise that the observed decrease in long-period ground motion for sites with shallow sediment depths might be caused by lower long-period site amplification as compared to sites with deeper sediments and a similar value of V_{S30}. We found that the data were sufficient to empirically constrain this trend.

The trend for $Z_{2.5}>3$ km, which is due presumably to 3-D basin response (e.g., Field 2000; Hruby and Beresnev 2003; Choi et al. 2005; Day et al. 2008, this volume), was based on too few data to empirically determine how this response could be extrapolated with respect to sediment depth and oscillator period. Instead, the basin term was constrained using the sediment depth term developed by Day et al. (2008, this volume) from theoretical 3-D ground motion simulations for the Los Angeles, San Gabriel, and San Fernando basins in southern California. The overall amplitude of this term was calibrated empirically from the regression analysis. These investigators also found that the simulated ground motions scaled strongly with sediment depth between depths of 1 and 3 km, whereas we did not find any trend in the residuals over this depth range. We believe that the predicted amplification between depths of 1 and 3 km is being preempted by other explanatory variables in our model. The most likely candidate is V_{S30}. For example, it is below a depth of 3 km that we found a strong correlation between $Z_{2.5}$ and V_{S30} in the PEER NGA database. It is also possible that the ground motion simulations are dominated by 1-D site response effects for sediment depths shallower than 3 km, which are adequately modeled by f_{site}. Like Field (2000), we found that PGA and short-period PSA were weakly correlated with basin depth.

We recognize that it might not always be possible to estimate the depth to the 2.5-km shear-wave velocity horizon, but that it might be possible to estimate the depths to shallower velocity horizons. In this case we recommend using the relationships and aleatory uncertainties developed by Campbell and Bozorgnia (2007) to estimate $Z_{2.5}$ from estimates of the depths to the 1 km $(Z_{1.0})$ or 1.5 km $(Z_{1.5})$ shear-wave velocity horizons.

LONG-PERIOD GROUND MOTION

As a result of the worldwide surge in the construction of tall buildings and seismically isolated structures in the last decade, there is an increasing need by engineers for reliable estimates of long-period ground motion. In response to this need, we have developed a ground motion model for the 5% damped relative response spectral displacement, $\text{SD}=(T/2\pi)^2\text{PSA}$, that we consider to be reasonably valid to $T=10$ s. We used this model for SD to develop a similar model for PGD based on the work of Faccioli et al. (2004). Although there have been attempts by others to develop empirical ground motion models for PGD and SD (e.g., Douglas 2006; Akkar and Bommer 2007), these models have generally been limited to periods of 5 s or less because of the contamination of the recordings with long-period noise. For this same reason, the number of recordings in our database with periods within the useable bandwidth fall off significantly for periods exceeding 4–5 s. For example, only 506 of the original 1561 recordings

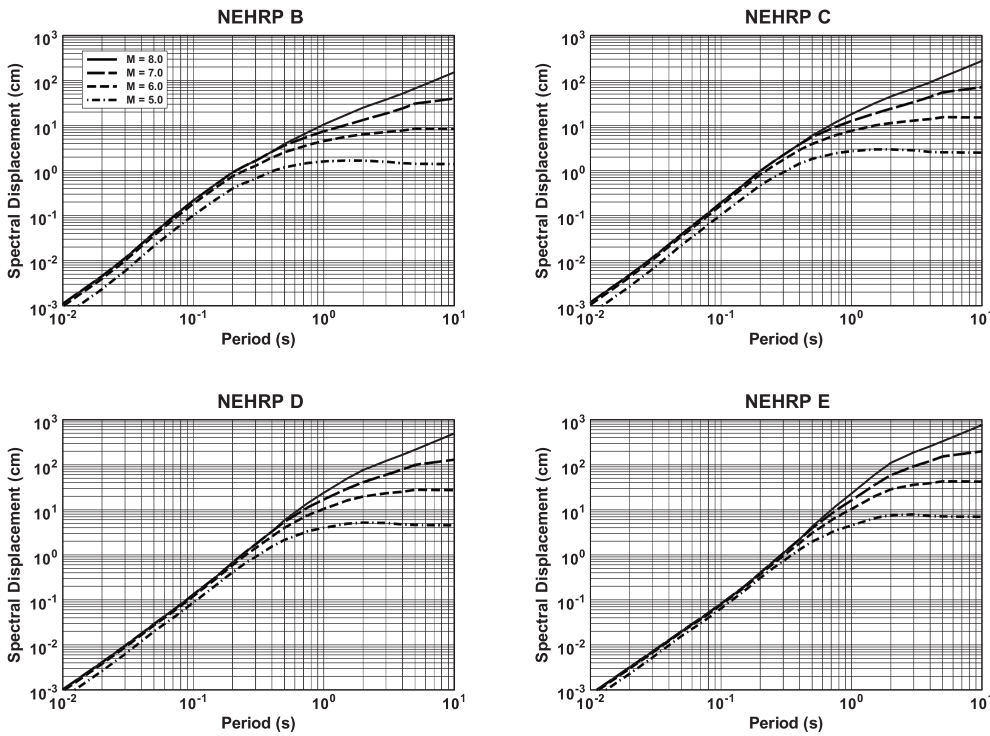

Figure 14. Predicted dependence of 5% damped relative displacement response spectra on moment magnitude (**M**) and 30-m shear-wave velocity (V_{S30}). The ground motion model is evaluated for **M**=5.0, 6.0, 7.0 and 8.0; V_{S30}=1070 m/s (NEHRP B), V_{S30}=525 m/s (NEHRP C), V_{S30}=255 m/s (NEHRP D) and V_{S30}=150 m/s (NEHRP E); $F_{RV}=F_{NM}=0$; $R_{RUP}=0$; and $Z_{2.5}$ =2 km.

from 21 of the original 64 earthquakes have spectral ordinates that fall within the useable bandwidth at T=10 s. The majority of these earthquakes have magnitudes in the range $6.5 \leq \mathbf{M} \leq 7.9$. Furthermore, nearly 70% of these recordings are from the Chi-Chi earthquake. This leads to an increasingly larger inter-event standard deviation as period increases.

In order to extend our model for SD to longer periods and smaller magnitudes, we constrained the magnitude scaling term using empirical observations and simple seismological theory (Atkinson and Silva 2000; Faccioli et al. 2004). Our resulting model is presented in Figure 14. The magnitude scaling term for PGD was constrained based on the observation that at small magnitudes SD at T=10 s (SD_{10}) is a reasonable approximation of PGD (Faccioli et al. 2004) and that at long periods, where SD_{10} has not yet reached an asymptotic value, near-source estimates of PGD can be constrained from geological observations of fault rupture displacement (T. Heaton, personal communication, 2006) using, for example, the magnitude scaling relations of Wells and Coppersmith (1994). Further justification of our long-period constraints is given in Campbell and Bozorgnia (2007).

CONCLUSIONS

The ground motion model presented in this paper, like the other models developed for the NGA project, represents a significant advancement in the empirical prediction of horizontal ground motion for use in engineering and seismology. Several of these models, including our own, incorporate in a single prediction equation such important features as period-dependent magnitude saturation, magnitude-dependent attenuation, style of faulting, depth of rupture, hanging-wall effects, shallow linear and nonlinear site response, basin response, and amplitude-dependent intra-event aleatory uncertainty. We, therefore, consider our NGA model to supersede our previous ground motion models (Campbell 1997; Campbell and Bozorgnia 2003). Figure 15, together with the additional comparisons between our NGA and previous ground motion models given in Campbell and Bozorgnia (2007), indicate that the impact of our new model on ground motion predictions at $\mathbf{M}<7$ is relatively small, which is due largely to the adoption of magnitude saturation effects to limit magnitude scaling and the use of conversion factors to correct for NEHRP B-C site conditions in our previous models.

We consider our new NGA model to be appropriate for estimating PGA, PGV, PGD and linear elastic response spectra ($T=0.01-10$ s) for shallow continental earthquakes occurring in western North America and other regimes of similar active tectonics (e.g., Campbell and Bozorgnia 2006; Stafford et al. 2008). The model is considered most reliable when evaluated for (1) $\mathbf{M}>4.0$; (2) $\mathbf{M}<8.5$ for strike-slip faulting, $\mathbf{M}<8.0$ for reverse faulting, and $\mathbf{M}<7.5$ for normal faulting; (3) $R_{RUP}=0-200$ km; (4) $V_{S30}=150-1500$ m/s or alternatively NEHRP site classes B, C, D and E; (4) $Z_{2.5}=0-10$ km; (5) $Z_{TOR}=0-15$ km; and (6) $\delta=15-90°$. The recommended upper magnitude limits represent an extrapolation of around one-half unit from the largest magnitude of each type of fault mechanism in our database. We believe that this extrapolation is justified given the magnitude scaling constraints imposed in the model. We have extended the applicable range of some of the explanatory variables beyond the limits of the data when we believe that the model has been adequately constrained either empirically or theoretically. This is particularly true of the ground motion models for PGD and SD for $T>4-5$ s, which were developed based partly on geological and seismological constraints (Campbell and Bozorgnia 2007). As a result, the values of PGD and SD predicted by our model serve as an initial attempt to provide realistic long-period constraints on these two important ground motion parameters.

We strongly suggest that the reader review the guidelines provided in Chapter 6 of Campbell and Bozorgnia (2007) before using our model. One of these items is worth repeating because of its potential importance in probabilistic seismic hazard analysis (PSHA) and other applications in which epistemic uncertainty is important. As a result of better data and mathematical constraints, the new set of NGA models does not necessarily quantify true epistemic uncertainty. It was the consensus amongst the NGA model developers that some additional epistemic uncertainty is warranted. Although it

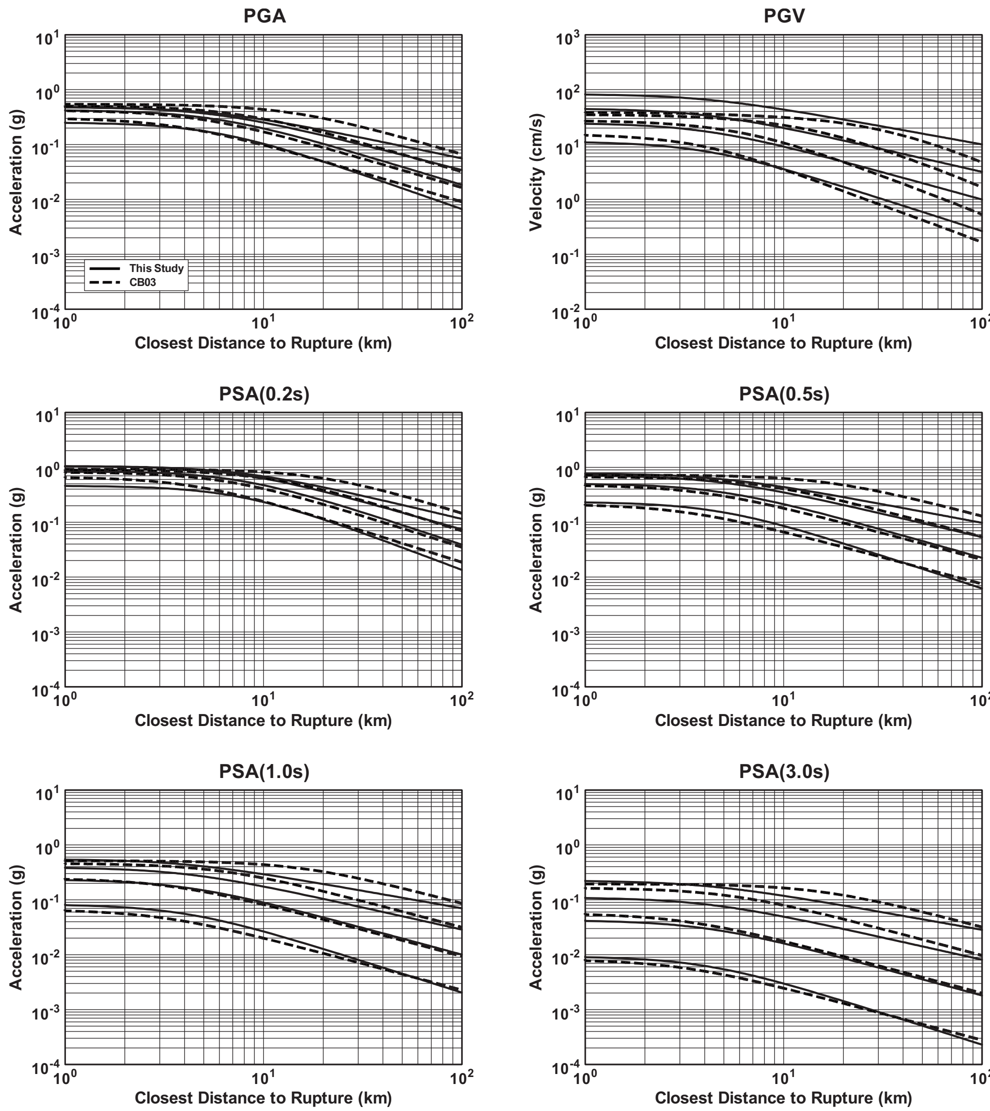

Figure 15. Comparison of predicted attenuation of ground motion from this study with that of Campbell (1997) for PGV and Campbell and Bozorgnia (2003) for PGA and PSA [CB03] for moment magnitudes of $\mathbf{M}=5.0$, 6.0, 7.0 and 8.0 (bottom to top). Explanatory variable settings for each of the models are listed in Table 7.3 of Campbell and Bozorgnia (2007).

was beyond the scope of the NGA project to develop such an epistemic uncertainty model, a simple model to account for the additional uncertainty in the estimation of near-source ground motion was proposed by the NGA project and adopted for use in the National Seismic Hazard Maps by Petersen et al. (2008).

ACKNOWLEDGMENTS

This study was sponsored by the Pacific Earthquake Engineering Research Center's (PEER's) Program of Applied Earthquake Engineering Research of Lifelines Systems supported by the California Department of Transportation, the California Energy Commission, and the Pacific Gas and Electric Company. This work made use of the Earthquake Engineering Research Centers Shared Facilities supported by the National Science Foundation, under award number EEC-9701568 through PEER. Any opinions, findings, and conclusions or recommendations expressed in this material are those of the authors and do not necessarily reflect those of the National Science Foundation. Numerous productive meetings and discussions with other NGA model developers and researchers are gratefully acknowledged. We would also like to thank Jon Stewart for providing us with additional insight into the effects of soil nonlinearity on aleatory uncertainty. The clarity of the paper was enhanced by the insightful comments of F. O. Strasser, J. J. Bommer, P. J. Stafford, and an anonymous reviewer.

REFERENCES

Abrahamson, N. A., and Silva, W. J., 1997. Empirical response spectral attenuation relations for shallow crustal earthquakes, *Seismol. Res. Lett.* **68**, 94–127.

——, 2008. Summary of the Abrahamson & Silva NGA ground-motion relations, *Earthquake Spectra* **24**, 67–97.

Abrahamson, N. A., and Youngs, R. R., 1992. A stable algorithm for regression analyses using the random effects model, *Bull. Seismol. Soc. Am.* **82**, 505–510.

Akkar, S., and Bommer, J. J., 2007. Prediction of elastic displacement response spectra in Europe and the Middle East, *Earthquake Eng. Struct. Dyn.* **36**, 1275–1301.

Ambraseys, N. N., Douglas, J., Sarma, S. K., and Smit, P. M., 2005. Equations for the estimation of strong ground motions from shallow crustal earthquakes using data from Europe and the Middle East: horizontal peak ground acceleration and spectral acceleration, *Bull. Earthquake Eng.* **3**, 1–53.

Atkinson, G. M., and Silva, W., 2000. Stochastic modeling of California ground motions, *Bull. Seismol. Soc. Am.* **90**, 255–274.

Baker, J. W., and Cornell, C. A., 2006. Which spectral acceleration are you using?, *Earthquake Spectra* **22**, 293–312.

Baturay, M. B., and Stewart, J. P., 2003. Uncertainty and bias in ground-motion estimates from ground response analyses, *Bull. Seismol. Soc. Am.* **93**, 2025–2042.

Bazzurro, P., and Cornell, C. A., 2004a. Ground motion amplification in nonlinear soil sites with uncertain properties, *Bull. Seismol. Soc. Am.* **94**, 2090–2109.

——, 2004b. Nonlinear soil-site effects in probabilistic seismic-hazard analysis, *Bull. Seismol. Soc. Am.* **94**, 2110–2123.

——, 2005. Erratum: ground motion amplification in nonlinear soil sites with uncertain properties, *Bull. Seismol. Soc. Am.* **95**, 2027.

Beyer, K., and Bommer, J. J., 2006. Relationships between median values and between aleatory variabilities for different definitions of the horizontal component of motion, *Bull. Seismol. Soc. Am.* **96**, 1512–1522.

Boore, D. M., 2005. Erratum: equations for estimating horizontal response spectra and peak acceleration from western North American earthquakes: a summary of recent work, *Seismol. Res. Lett.* **76**, 368–369.

Boore, D. M., Joyner, W. B., and Fumal, T. E., 1997. Equations for estimating horizontal response spectra and peak acceleration from western North American earthquakes: a summary of recent work, *Seismol. Res. Lett.* **68**, 128–153.

Boore, D. M., Watson-Lamprey, J., and Abrahamson, N., 2006. Orientation-independent measures of ground motion, *Bull. Seismol. Soc. Am.* **96**, 1502–1511.

Borcherdt, R. D., 1994. Estimates of site-dependent response spectra for design (methodology and justification), *Earthquake Spectra* **10**, 617–653.

Bozorgnia, Y., Hachem, M. M., and Campbell, K. W., 2006. Attenuation of inelastic and damage spectra, in *Proceedings, Eighth National Conference on Earthquake Engineering*, Paper No. 1127, San Francisco, 10 pp.

Campbell, K. W., 1981. Near-source attenuation of peak horizontal acceleration, *Bull. Seismol. Soc. Am.* **71**, 2039–2070.

——, 1997. Empirical near-source attenuation relationships for horizontal and vertical components of peak ground acceleration, peak ground velocity, and pseudo-absolute acceleration response spectra, *Seismol. Res. Lett.* **68**, 154–179.

Campbell, K. W., and Bozorgnia, Y., 2003. Updated near-source ground motion (attenuation) relations for the horizontal and vertical components of peak ground acceleration and acceleration response spectra, *Bull. Seismol. Soc. Am.* **93**, 314–331.

——, 2006. Next generation attenuation (NGA) empirical ground motion models: can they be used in Europe?, in *Proceedings, First European Conference on Earthquake Engineering and Seismology*, Paper No. 458, Geneva, 10 pp.

——, 2007. *Campbell-Bozorgnia NGA ground motion relations for the geometric mean horizontal component of peak and spectral ground motion parameters*, PEER Report No. *2007/02*, Pacific Earthquake Engineering Research Center, University of California, Berkeley, 238 pp.

Chiou, B. S.-J., and Youngs, R. R., 2008. An NGA model for the average horizontal component of peak ground motion and response spectra, *Earthquake Spectra* **24**, 173–215.

Choi, Y., and Stewart, J. P., 2005. Nonlinear site amplification as function of 30 m shear wave velocity, *Earthquake Spectra* **21**, 1–30.

Choi, Y., Stewart, J. P., and Graves, R. W., 2005. Empirical model for basin effects that accounts for basin depth and source location, *Bull. Seismol. Soc. Am.* **95**, 1412–1427.

Collins, N., Graves, R., Ichinose, G., and Somerville, P., 2006. *Ground motion attenuation relations for the Intermountain West*, Final report to U. S. Geological Survey, Award No. 05HQGR0031.

Day, S. M., Graves, R., Bielak, J., Dreger, D., Larsen, S., Olsen, K. B., Pitarka, A., and Ramirez-Guzman, L., 2008. Model for basin effects on long-period response spectra in southern California, *Earthquake Spectra* **24**, 257–277.

Douglas, J., 2006. *Errata of and Additions to 'Ground Motion Estimation Equations 1964–2003'*, BRGM/RP-54603-FR, Bureau de Recherches Géologiques et Minières (BRGM), Orléans, France, 103 pp.

Field, E. H., 2000. A modified ground-motion attenuation relationship for southern California that accounts for detailed site classification and a basin-depth effect, *Bull. Seismol. Soc. Am.* **90**, S209–S221.

Faccioli, E., Paolucci, R., and Rey, J., 2004. Displacement spectra at long periods, *Earthquake Spectra* **20**, 347–376.

Frankel, A. D., 2007. Do the next generation attenuation relations make physical sense?, Abstract, *Seismol. Res. Lett.* **78**, 287.

Hruby, C. E., and Beresnev, I. A., 2003. Empirical corrections for basin effects in stochastic ground motion prediction based on Los Angeles basin analysis, *Bull. Seismol. Soc. Am.* **93**, 1679–1690.

Kwok, A. O., and Stewart, J. P., 2006. Evaluation of the effectiveness of theoretical 1D amplification factors for earthquake ground-motion prediction, *Bull. Seismol. Soc. Am.* **96**, 1422–1436.

Petersen, M., Frankel, A., Harmsen, S., Mueller, C., Haller, K., Wheeler, R., Wesson, R., Zeng, Y., Boyd, O., Perkins, D., Luco, N., Field, E., Wills, C., and Rukstales, K., 2008. *Documentation for the 2008 update of the United States national seismic hazard maps*, U.S. Geological Survey Open-File Report *2008-1128*.

Power, M., Chiou, B., Abrahamson, N., Bozorgnia, Y., Shantz, T., and Roblee, C., 2008. An overview of the NGA project, *Earthquake Spectra* **24**, 3–21.

Schmedes, J., and Archuleta, R. J., 2007. Oversaturation of peak ground velocity along strike slip faults, Abstract, *Seismol. Res. Lett.* **78**, 272.

Silva, W. J., Li, S., Darragh, R. B., and Gregor, N., 1999. *Surface Geology Based Strong Motion Amplification Factors for the San Francisco Bay and Los Angeles Areas*, Report to Pacific Earthquake Engineering Research Center (PEER), University of California, Berkeley.

Silva, W. J., Darragh, R. B., Gregor, N., Martin, G., Abrahamson, N. A., and Kircher, C., 2000. *Reassessment of Site Coefficients and Near-Fault Factors for Building Code Provisions*, Final report to U. S. Geological Survey, Award No. 98HQGR1010.

Stafford, P. J., Strasser, F. O., and Bommer, J. J., 2008. An evaluation of the applicability of the NGA models to ground-motion prediction in the Euro-Mediterranean region, *Bull. Earthquake Eng.* **6**, 149–177.

Stewart, J. P., Liu, A. H., and Choi, Y., 2003. Amplification factors for spectral acceleration in tectonically active regions, *Bull. Seismol. Soc. Am.* **93**, 332–352.

Stewart, J. P., and Goulet, C. A., 2006. Comment on "Nonlinear Soil-Site Effects in Probabilistic Seismic-Hazard Analysis" by Paolo Bazzurro and C. Allin Cornell, *Bull. Seismol. Soc. Am.* **96**, 745–747.

Walling, M., Silva, W., and Abrahamson, N., 2008. Nonlinear site amplification factors for constraining the NGA models, *Earthquake Spectra* **24**, 243–255.

Watson-Lamprey, J. A., and Boore, D. M., 2007. Beyond *SaGMRotI*: conversion to Sa_{Arb}, Sa_{SN}, and Sa_{MaxRot}, *Bull. Seismol. Soc. Am.* **97**, 1511–1524.

Wells, D. L., and Coppersmith, K. J., 1994. New empirical relationships among magnitude, rupture length, rupture width, rupture area, and surface displacement, *Bull. Seismol. Soc. Am.* **84**, 974–1002.

(Received 4 July 2007; accepted 4 January 2008)